Lifetime measurements of $N \simeq 20$ phosphorus isotopes using the AGATA γ-ray tracking spectrometer

L. Grocutt,[1] R. Chapman,[1,*] M. Bouhelal,[2] F. Haas,[3,4] A. Goasduff,[5] J. F. Smith,[1] S. Courtin,[3,4] D. Bazzacco,[6,7] T. Braunroth,[8] L. Capponi,[1,9] L. Corradi,[5] X. Derkx,[1] P. Desesquelles,[10,11] M. Doncel,[12,13] E. Fioretto,[5] A. Gottardo,[5] V. Liberati,[1] B. Melon,[14] D. Mengoni,[6,7] C. Michelagnoli,[15] T. Mijatović,[16] V. Modamio,[5] G. Montagnoli,[6] D. Montanari,[6] K. F. Mulholland,[1] D. R. Napoli,[5] C. Petrache,[17] A. Pipidis,[5] F. Recchia,[6] E. Sahin,[5,18] P. P. Singh,[19] A. M. Stefanini,[5] S. Szilner,[5,16] and J. J. Valiente-Dobón[5]

[1]*School of Computing, Engineering, and Physical Sciences, University of the West of Scotland, Paisley, PA1 2BE, United Kingdom and the Scottish Universities Physics Alliance (SUPA)*

[2]*Laboratoire de Physique Appliquée et Théorique, Université Larbi Tébessi, Tébessa, Algeria*

[3]*IPHC, Université de Strasbourg, Strasbourg, F-67037, France*

[4]*CNRS, UMR7178, Strasbourg, F-67037, France*

[5]*Istituto Nazionale di Fisica Nucleare, Laboratori Nazionali di Legnaro, I-35020 Legnaro, Padova, Italy*

[6]*Dipartimento di Fisica e Astronomia, Universitá degli Studi di Padova, I-35131 Padova, Italy*

[7]*Istituto Nazionale di Fisica Nucleare, Sezione di Padova, I-35131 Padova, Italy*

[8]*Institute für Kernphysik der Universitat zu Köln, D-50937 Köln, Germany*

[9]*Extreme Light Infrastructure Nuclear Physics/IFIN-HH, Bucharest-Magurele, RO-077125, Romania*

[10]*Centre des Sciences Nucléaires et des Sciences de la Matières (CSNSM), Université Paris-Sud, France*

[11]*CNRS-IN2P3, Université Paris-Saclay, Bâtiment 104, 15 rue Clemenceau, F91405 Orsay Cédex, France*

[12]*Laboratorio de Radiaciones Ionizantes, Universidad de Salamanca, E-37008 Salamanca, Spain*

[13]*Department of Physics, Oliver Lodge Laboratory, University of Liverpool, Liverpool L69 7ZE, United Kingdom*

[14]*Dipartimento di Fisica e Astronomia, Universitá di Firenze, IT-50019, Sesto Fiorentino (Firenze), Italy*

[15]*Institut Laue-Langevin, B.P. 156, F-38042 Grenoble Cédex 9, France*

[16]*Ruder Bošković Institute, Zagreb, Croatia*

[17]*Centre de Sciences Nucléaires et Sciences de la Matière, CNRS/IN2P3, Université Paris-Saclay, Bâtiment 104-108, 91405 Orsay, France*

[18]*Department of Physics, University of Oslo, P.O. Box 1048, Blindern, N-0316, Oslo, Norway*

[19]*Department of Physics, Indian Institute of Technology Ropar, Rupnagar, Punjab 140 001, India*

(Received 23 May 2019; revised manuscript received 12 September 2019; published 13 December 2019)

Lifetimes of excited states of the phosphorus isotopes $^{33,34,35,36}_{15}$P have been measured by using the differential recoil-distance method. The isotopes of phosphorus were populated in binary grazing reactions initiated by a beam of ^{36}S ions of energy 225 MeV incident on a thin ^{208}Pb target mounted in the Cologne plunger apparatus. The combination of the PRISMA magnetic spectrometer and an early implementation of the AGATA γ-ray tracking array was used to detect γ rays in coincidence with projectile-like nuclear species. Lifetime measurements of populated states were made within the range from about 1 to 100 ps. The number of states for which lifetime measurements were possible was limited by statistics. For ^{33}P, lifetime limits were determined for the first $3/2^+$ and $5/2^+$ states at 1431 and 1848 keV, respectively; the results are compared with previous published lifetime values. The lifetime of the first 2^+ state of ^{34}P at 429 keV was determined and compared with earlier measurements. For ^{35}P, the states for which lifetimes, or lifetime limits, were determined were those at 2386, 3860, 4101, and 4493 keV, with J^π values of $3/2^+$, $5/2^+$, $7/2^-_1$, and $7/2^-_2$, respectively. There have been no previous published lifetimes for states in this nucleus. A lifetime was measured for the stretched $\pi(1f_{7/2}) \otimes \nu(1f_{7/2})\, J^\pi = (7^+)$ state of ^{36}P at 5212 keV and a lifetime limit was established for the stretched $\pi(1d_{3/2}) \otimes \nu(1f_{7/2})\, J^\pi = (5^-)$ state at 2030 keV. There are no previously published lifetimes for states of ^{36}P. Measured lifetime values were compared with the results of state-of-the-art shell-model calculations based on the PSDPF effective interaction. In addition, measured branching ratios, published mixing ratios, and electromagnetic transition rates, where available, have been compared with shell-model values. In general, there is good agreement between experiment and the shell model; however there is evidence that the shell-model values of the $M1$ transition rates for the $3/2^+_1 \rightarrow 1/2^+$ (ground state) and $5/2^+_1 \rightarrow 3/2^+_1$ transitions in ^{33}P underestimate the experimental values by a factor between 5 and 10. In ^{35}P there are some disagreements between experimental and shell-model values of branching ratios for the first and second excited $7/2^-$ states. In particular, there is a serious disagreement for the decay characteristics of the second $7/2^-$ state at 4493 keV, for which the

*robert.chapman@uws.ac.uk

shell-model counterpart lies at 4754 keV. In this case, the shell-model competing electromagnetic decay branches are dominated by $E1$ and $M1$ transitions.

DOI: 10.1103/PhysRevC.100.064308

I. INTRODUCTION

The present paper is concerned with the measurement of lifetimes of excited states of nuclei in the *sd*-shell near the $N = 20$ shell closure using the differential recoil-distance method [1–3]. The nuclei of interest were populated in binary grazing reactions initiated by the interaction of 225-MeV ^{36}S ions with a thin target of ^{208}Pb. The nuclear species observed in the reaction have previously been studied in an experiment carried out at the INFN Legnaro National Laboratory using the same beam-target combination at a beam energy of 215 MeV. The earlier work used the combination of PRISMA [4,5], a large-solid-angle magnetic spectrometer to identify the projectile-like nuclear species, and CLARA [6], an array of escape-suppressed Ge γ-ray detectors to measure the γ-ray decay of the populated levels. The previous published works from the experiment have involved studies of the neutron-rich isotopes ^{33}Si [7], ^{36}Si [8], ^{34}P [9], ^{35}P [9], ^{36}P [9], ^{37}P [9,10], ^{38}P [9], ^{37}S [11], ^{39}S [12], ^{40}S [13], ^{41}S [14], and ^{38}Cl [15]. In addition, the level structures of other populated isotopes of silicon [16], phosphorus [17], sulphur [16], and chlorine [18] were investigated. The studies were mainly concerned with the role of negative-parity intruder orbitals in the structure of neutron-rich nuclei on the periphery of the island of inversion, which is centered on ^{32}Mg, and on the description of such nuclei using state-of-the-art shell-model calculations [19]. Binary grazing and deep-inelastic reactions have been used extensively over the last few decades to study the structure of neutron-rich nuclei over a wide range of nuclear masses. The coupling of large-solid-angle magnetic spectrometers to arrays of escape-suppressed Ge detectors in studies of this type (see e.g., Refs. [20–22]) has represented a very significant experimental advance in relation to earlier techniques which exploited large arrays of escape-suppressed Ge γ-ray detectors but no particle identification; see e.g., Broda *et al.* [23], Fornal *et al.* [24], and Lee *et al.* [25]. Here, we extend the study of the nuclear structure of a few of the previously studied *sd*-shell nuclei through the measurement of nuclear lifetimes and a comparison is made with the results of state-of-the art shell-model calculations based on the PSDPF effective interaction [26], also presented here. Shell-model calculations of the electromagnetic transition probabilities of excited states strongly depend on, and are sensitive to, the details of the wave functions of the two states involved in the transition. The assumed configuration space used in such calculations, the shell-model interaction, and the effective nucleon charges will also have a direct effect on the calculated values.

Here, lifetimes of populated states were measured using a differential plunger [1] in combination with the PRISMA magnetic spectrometer [4,5] and an early implementation of the AGATA γ-ray tracking array [27]. The number of states for which lifetime measurements, or lifetime limits, have been made has been severely limited by the statistics of the experiment. Nuclei for which the experimental data allow the measurements of lifetimes to be made lie close to neutron number 20. In particular, the isotopes of phosphorus for which lifetimes of excited states, or lifetime limits, have been established are ^{33}P, ^{34}P, ^{35}P, and ^{36}P with neutron numbers $N = 18$–21, respectively. Lifetime measurements from the same experiment for the isotopes of sulfur with mass numbers $A = 35$–38, and the isotopes of Si with $A = 32$–34 will be presented in future publications [28,29].

II. EXPERIMENT

Yrast and near-yrast states of the final nuclei were populated using binary grazing reactions produced in the interaction of a 225-MeV (6 MeV/u) beam of $^{36}S^{9+}$ ions of average current 1 pnA, delivered by the Tandem-ALPI accelerator complex at the INFN Legnaro National Laboratory, Italy, with a thin ^{208}Pb target. The stretched Pb target of thickness 1 mg cm^{-2}, and isotopically enriched to 99.7% in ^{208}Pb, was deposited onto a 1 mg cm^{-2} Nb backing foil and mounted onto the Köln differential plunger [1,2], with the niobium backing facing the incident beam. The beam energy at the center of the Pb target was 215 MeV, the same energy as that which was used in the earlier experiment, to which reference has been made above. The degrader foil, used in the differential plunger apparatus to reduce the velocity of projectile-like nuclei after they leave the Pb target, consisted of a 3 mg cm^{-2} Nb foil mounted at a short distance downstream from the target. The distance between the Pb target and degrader foil was adjusted and controlled by a piezo-electric feedback system developed at the University of Cologne [30]. As the recoiling projectile-like nucleus moves through the plunger towards the entrance to PRISMA, the probability of γ-ray emission before or after passage through the degrader foil depends on the distance between target and degrader foils, the effective lifetime of the decaying state, and the velocity of the emitting nucleus. If the lifetime is comparable to the flight time of the nucleus between the Pb target and degrader, two photopeak components are observed in the γ-ray energy spectrum for each γ-ray transition, corresponding to the different Doppler shifts associated with recoil velocities before and after passage through the degrader. For the exit channel corresponding to one proton transfer (^{35}P as the final nucleus), for example, the v/c values of the recoiling nucleus before and after passage through the degrader are 10.0% and 9.4%, respectively. With the present experimental setup, lifetime measurements from about 1 ps to about 100 ps are possible.

The plunger device was placed in the reaction chamber of PRISMA [4,5] with its axis at 14° with respect to the PRISMA optical axis. Projectile-like fragments, produced in binary grazing reactions, pass through the degrader foil and into the PRISMA magnetic spectrometer where they are detected and identified. PRISMA was positioned at 56° with respect to the beam axis, covering a range of angles including the grazing

angle of the reaction. The PRISMA spectrometer consists of a quadrupole singlet and a dipole magnet separated by 60 cm. The (x, y) coordinates and time information of an ion entering the spectrometer are measured using a position-sensitive microchannel plate (MCP) detector [31] placed at 25 cm from the target. Following the passage of each ion through the magnetic elements, the coordinates of the trajectory and time information are measured again at the focal plane of the spectrometer by using a ten-element 100-cm-long multiwire parallel-plate avalanche counter (MWPPAC) [32]. The position resolution of the MCP and MWPPAC is 1 mm in the horizontal (dispersive) direction and the time resolution of the MCP and MWPPAC combination is about 300 ps. Finally, the ions are stopped in a 10×4 element ionization chamber (IC) used for energy-loss measurements, ΔE, and total energy E measurements [31,32]. For each ion detected in PRISMA, the above measurements enable a determination of the atomic number Z, the mass number A, the ion charge state, and the time of flight, thereby allowing an unambiguous identification of each detected projectile-like nucleus. PRISMA has a solid angle of 80 msr, a momentum acceptance of $\pm 10\%$, and a mass resolution of $1/300$ via time-of-flight measurements. Reconstruction of the trajectory of each ion through the spectrometer together with the time-of-flight measurement was used to establish the velocity vector of each ion on an event-by-event basis, essential for lifetime measurements by the differential recoil-distance technique, which relies on an accurate knowledge of the velocity of the projectile-like nucleus and the distance between target and degrader foils.

The associated deexcitation γ rays emitted by the recoiling nuclei were detected by the AGATA demonstrator array [33]. This new state-of-the-art germanium detector array was composed of five triple-cluster modules positioned 18 cm from the reaction target and covering backward angles from 135° to 175°. The corresponding simulated full-absorption efficiency for γ rays of energy 1 MeV is about 7%. Digitized signal pulses from the 36-fold segmented germanium crystals were compared with a data base of simulated detector responses using a pulse-shape analysis algorithm [34] to determine the loci of γ-ray interactions in the detector crystals. The resulting position resolution is better than 5 mm full width at half maximum (FWHM). The application of a γ-ray tracking algorithm [35] resulted in the energies of individual γ rays. Energies and interaction positions of γ rays were stored in list mode with a time stamp, which permitted a correlation to be established between γ-ray events and the associated projectile-like reaction products identified at the focal plane of PRISMA. To reduce the counting rate from ^{208}Pb x rays, a lead absorber of thickness 2 mm was placed between AGATA and the reaction chamber. In total, five different distances, 7, 20, 35, 65, and 120 μm, between the target and the degrader foils of the Köln differential plunger were used during the experiment. The experiment ran for nine days, with between one and two days of data accumulated for each distance. The data-acquisition trigger was provided by timing signals from the large area multiwire parallel plate avalanche counter (MWPPAC) at the focal plane of PRISMA. Doppler correction of γ-ray energies was performed on an event-by-event basis. A relative photopeak efficiency calibration for the AGATA array was carried out using radioactive sources of ^{152}Eu and ^{133}Ba.

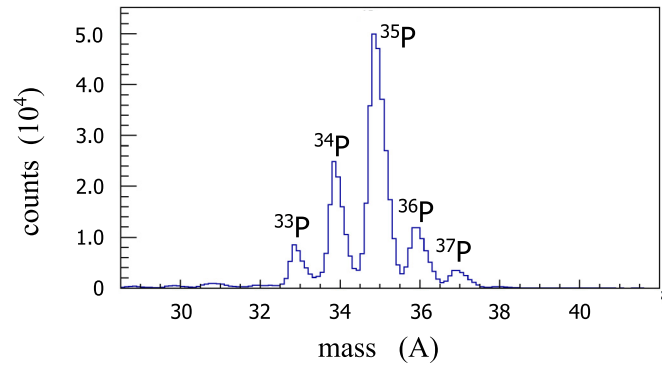

FIG. 1. The mass spectrum of phosphorus ions detected at the focal plane of the PRISMA spectrometer in coincidence with γ rays.

In summary, lifetime measurements using the recoil-distance method have exploited the powerful combination of a large-acceptance magnetic spectrometer, PRISMA, and a high-efficiency γ-ray tracking array, AGATA, which results in good reaction-channel selection and precise Doppler correction of γ-ray energy spectra.

III. RESULTS AND DISCUSSION

In the present experiment, a wide range of nuclear species, from Mg ($Z = 12$) to Ca ($Z = 20$), was identified at the focal plane of PRISMA. Here, we focus on a discussion of those isotopes of phosphorus for which reaction yields were sufficiently large for the measurement of nuclear lifetimes to be made using the present experimental setup.

A. The isotopes of phosphorus

The mass spectrum of Fig. 1 shows that the phosphorus isotopes with mass numbers $33 \leqslant A \leqslant 37$, i.e., up to six neutrons from stability, were successfully populated in the present work. The measured mass resolution is $1/140$. There is weak population of phosphorus isotopes outside this mass range and the consequent poor statistics do not allow γ-ray spectroscopy measurements to be performed for these isotopes. The most strongly populated isotope is ^{35}P, corresponding to one proton transfer. For the isotope ^{37}P, the yield was not sufficient for lifetime measurements to be made. A mass gate of suitable location and width was used to produce a one-dimensional γ-ray spectrum corresponding to the particular isotope of interest. Experimental results for the isotopes of phosphorus for which lifetimes, or lifetime limits, have been established here; namely ^{33}P, ^{34}P, ^{35}P, and ^{36}P will now be presented together with the results of state-of-the-art shell-model calculations of the electromagnetic decay properties of the nuclear states involved. Where previous lifetimes have been reported, they will be compared with the results of the present work. In those cases for which the accuracy of the published lifetime value is significantly better than that from the present experiment, the results of the current work, including the results of shell-model calculations, will nevertheless be presented in

the interests of completeness. The $(0+1)\hbar\omega$ states in the phosphorus isotopes with $A = 33$–36 are described here with the PSDPF interaction [26]. This shell-model calculation has a ^{4}He core and uses the full *p-sd-pf* model space; it is built on existing interactions for the major shells with adjustments of the cross-shell parameters. The positive-parity states are essentially obtained using the USDB Hamiltonian, developed by Brown and Richter [36], which is included in the PSDPF interaction. Excitation of one nucleon is allowed across a major shell, from the *sd*-shell to the *pf*-shell in the present case. In the calculation of $E2$ and $E3$ electromagnetic transition probabilities, effective charges of $e_{\rm eff}(p) = 1.36e$ and $e_{\rm eff}(n) = 0.45e$ were used while, for the calculation of $B(M1)$ and $B(M2)$ transition probabilities, the effective spin and orbital g-factors of $g_{\nu s}^{\rm eff} = -3.55$, $g_{\nu \ell}^{\rm eff} = -0.09$, $g_{\pi s}^{\rm eff} = 5.150$, and $g_{\pi \ell}^{\rm eff} = 1.159$ were adopted [37]. Shell-model calculations were performed using the NATHAN code [19,38,39].

B. Lifetimes in ^{33}P

Within the context of the simple shell model, the ground state of ^{33}P, with $Z = 15$ and $N = 18$, has the configuration $\pi(1d_{5/2})^6(2s_{1/2})^1 \otimes \nu(1d_{5/2})^6(2s_{1/2})^2(1d_{3/2})^2$. The ground-state J^π value is therefore expected to be $1/2^+$. The experimental ground state J^π value of $1/2^+$ is based on the results of an experiment which studied the two-neutron transfer reaction, ^{31}P$(t, p)^{33}$P [40]. Low-lying $J^\pi = 3/2^+$ and $5/2^+$ excited states correspond to the promotion of the odd proton to the $1d_{3/2}$ orbital and to the promotion of a $1d_{5/2}$ proton to the $2s_{1/2}$ orbital, respectively. The J^π values of the two states at excitation energies of 1435(6) and 1843(4) keV, respectively, were established by using the proton-pickup reaction ^{34}S$(d,^3$He$)^{33}$P [41], with a polarized deuteron beam. The population of the $3/2^+$ state in proton pickup from the ^{34}S ground state, with a spectroscopic factor of $C^2S = 0.63$, indicates that the proton $1d_{3/2}$ orbital in the ground state of ^{34}S is not empty, as would be expected in a simple shell-model picture. Higher-lying negative-parity states correspond to the promotion of a nucleon into the fp shell. The first negative-parity state is at an excitation energy of 4226 keV [42]. Shell-model wave functions of the states for which lifetimes have been measured will be discussed later. Lifetime measurements of the first two excited states of ^{33}P were made by Currie *et al.* [43] in the late 1960s. The ^{30}Si$(\alpha, p\gamma)^{33}$P reaction was used to populate excited states of the final nucleus; lifetimes were determined by using the Doppler-shift attenuation method, with NaI(Tl) γ-ray detectors. Experiments carried out in the early 1970s by Poletti *et al.* [44] and Wagner *et al.* [45] used the ^{31}P$(t, p\gamma)^{33}$P two-neutron transfer reaction, and the γ decay of populated states was studied with Ge(Li) detectors; the work resulted in a more precise determination of energies and lifetimes of excited states of ^{33}P.

The γ-ray spectrum measured in coincidence with ^{33}P ions detected and identified at the focal plane of the PRISMA spectrometer is shown in Fig. 2. All of the labeled γ-ray peaks were previously identified in the earlier experiment carried out at the INFN Legnaro National Laboratory, referred to above [9,17]. Figure 3 presents the level scheme of ^{33}P from that study. In the present work, lifetime measurements have been made for the first two excited states at 1431 and 1848 keV, with J^π values of $3/2^+$ and $5/2^+$, respectively.

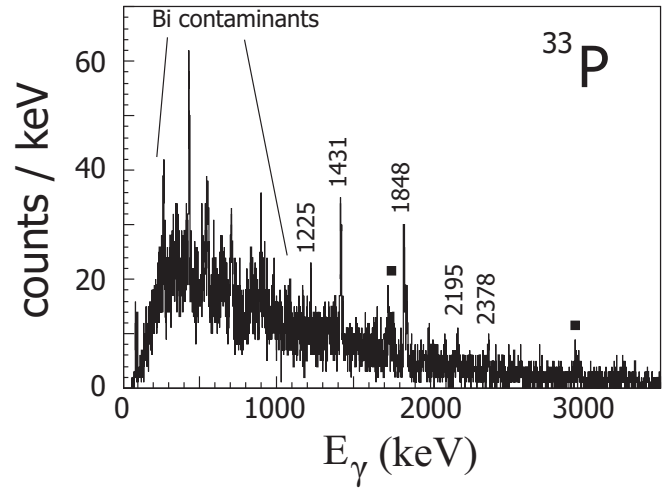

FIG. 2. γ-ray-singles energy spectrum observed in coincidence with ^{33}P ions detected at the focal plane of PRISMA. The target-like photopeaks correspond to γ rays emitted from $^{209-211}$Bi. The photopeaks separately labeled with the symbol ■ correspond to γ rays from the complementary unobserved fragment, ^{209}Bi.

C. Lifetime of the first-excited $J^\pi = 3/2^+$ state of ^{33}P at 1431 keV

Figure 4 presents a section of the measured γ-ray spectra for target-degrader distances of 7 and 120 μm and shows the two components of the photopeak which correspond to the 1431 keV $3/2^+$ to $1/2^+$ (ground-state) transition. Gaussian fits to the two components of the photopeak are also presented. The statistics are poor and the resulting lifetime has a large associated statistical uncertainty. The lifetime of the 3626-keV feeding state has been measured as $\tau = 0.11 \pm 0.02$ ps [45], which is less than the shortest lifetime that can be measured with the present experimental setup. Feeding from the $7/2_1^+$ state, although of a significant intensity, is therefore expected to have little effect on the measured lifetime of the $3/2_1^+$ state. The relative intensity of the 2195- and 1431-keV transitions is $I_\gamma(2195\ \text{keV})/I_\gamma(1431\ \text{keV}) = 0.33(3)$ [17]. When the 417-keV $5/2_1^+$ to $3/2_1^+$ branch, unobserved in the present work, is taken into account [42], the feeding of the $3/2_1^+$ state from above, through the 2195- and 417-keV transitions, accounts for 44% of the intensity of the 1431-keV transition. The statistical uncertainty in the value of lifetime based on the present data is large and, consequently, only an upper limit to the lifetime of <2 ps is given in Table I. As noted earlier, the lifetime of the first $3/2^+$ state has previously been measured using the Doppler-shift attenuation method by Currie *et al.* [43], Poletti *et al.* [44], and Wagner *et al.* [45]. The three independent values of 0.79 ± 0.23, 0.70 ± 0.15, and 0.6 ± 0.1 ps, respectively, are consistent within the quoted errors. The accepted value of lifetime is 0.62 ± 0.10 ps [42]. The present lifetime limit is consistent with the published lifetime value; it is included here for completeness and to allow the presentation of a lifetime calculated with a

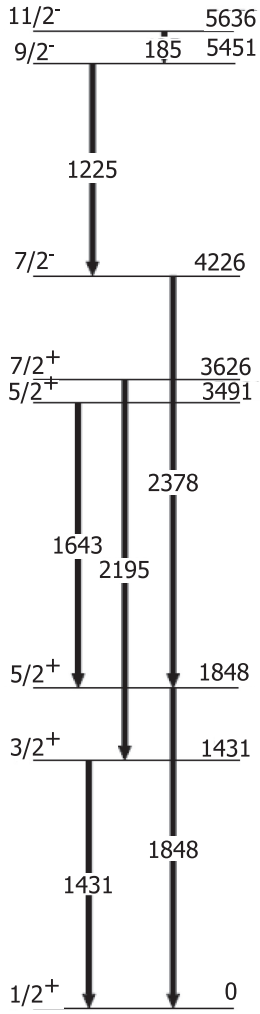

FIG. 3. Level scheme of ^{33}P from the earlier ^{36}S + ^{208}Pb experiment [17].

state-of-the-art shell-model interaction (PSDPF), discussed earlier, and its comparison with the best available lifetime value. The measurement here of an upper limit to the lifetime, which is both short and in agreement with the previously measured value, is consistent with a small contribution to the measured lifetime of the state from the unobserved side feeding. However, as will be explained later, the analysis method used for the states studied here will result in the suppression of contributions to the measured lifetime from both known feeding transitions and unobserved side-feeding transitions. Table I presents a summary of the experimental

TABLE I. Experimental and shell-model values of excitation energies and lifetimes of states in ^{33}P. Adopted lifetimes are from Ref. [42].

J^π	E (expt.) (keV)	E (SM) (keV)	τ (present) (ps)	τ (adopted) (ps)	τ (SM) (ps)
$3/2^+$	1431	1441	<2	0.62(10)	1.97
$5/2^+$	1848	1905	<2	1.11(16)	1.04

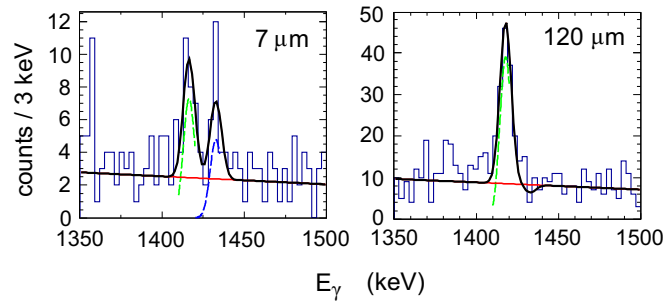

FIG. 4. Section of the measured γ-ray spectra for target-degrader distances of 7 and 120 μm which shows the two components of the 1431-keV photopeak corresponding to the $3/2_1^+$ to $1/2^+$ (ground-state) transition in ^{33}P. The black curve corresponds to a fit to the data (Gaussian peaks plus linear background). Background-subtracted photopeaks are shown in green (corresponding to γ-ray emission between the target and absorber) and in blue (corresponding to γ-ray emission after the decaying nucleus has passed through the degrader foil).

and shell-model energies and lifetimes for the two states of interest here in ^{33}P. For the first $3/2^+$ state, there is excellent agreement between experimental (1431 keV) and shell-model (1441 keV) level energies. Although the shell-model lifetime (1.97 ps) lies outside the previously published experimental values, it is of the same order of magnitude and is consistent with the lifetime limit established in the present work. In the calculation of shell-model lifetimes, experimental transition energies have been used rather than those from shell-model calculations, and this practice will be adopted throughout the paper.

Table II presents the other electromagnetic decay properties of the $3/2_1^+$ state. The 1431-keV $3/2_1^+ \rightarrow 1/2^+$ transition is a mixed $M1/E2$ transition with a measured mixing ratio [$\delta^2 = \lambda(E2)/\lambda(M1)$, where λ is the electromagnetic decay probability] of $\delta = -0.62 \pm 0.15$ [42]. However, the $M1$ transition, when it proceeds by a proton moving from the $1d_{3/2}$ to the $2s_{1/2}$ orbital, is $\Delta\ell$ forbidden [46]. The experimental $B(M1; 3/2_1^+ \rightarrow 1/2^+)$ value corresponding to the accepted lifetime quoted above is 0.013 ± 0.003 W.u. and the $B(E2; 3/2_1^+ \rightarrow 1/2^+)$ value is 10 ± 4 W.u. The small $B(M1)$ value is consistent with the transition being $\Delta\ell$ forbidden.

The first $1/2^+$ and $3/2^+$ states do not have a pure single-proton wave function and this is especially so for the $3/2_1^+$ state. As expected, the ground-state wave function of ^{33}P has, as the largest component (52%) in its wave function, the configuration

$$\pi(1d_{5/2})^6(2s_{1/2})^1 \otimes \nu(1d_{5/2})^6(2s_{1/2})^2(1d_{3/2})^2,$$

in which the odd proton occupies the $2s_{1/2}$ shell-model orbital. The 1431-keV $J^\pi = 3/2_1^+$ state has, as the main component (33%), the configuration

$$\pi(1d_{5/2})^6(2s_{1/2})^0(1d_{3/2})^1 \otimes \nu(1d_{5/2})^6(2s_{1/2})^2(1d_{3/2})^2.$$

Shell-model calculations based on the PSDPF interaction were used to predict the electromagnetic decay properties of the $3/2_1^+$ state, see Table II. The calculated values are $B(M1; 3/2_1^+ \rightarrow 1/2^+) = 0.0041\mu_N^2$ (0.0023 W.u.) and

TABLE II. Experimental and shell-model values of electromagnetic decay properties of states in ^{33}P. The experimental values are those of the Nuclear Data Sheets evaluation of Chen and Singh [42].

J^π	E (expt.) (keV)	E_f, J_f^π (keV)	BR (expt.) (%)	BR (SM) (%)	δ (expt.)	$\lvert\delta\rvert$ (SM)	$B(M1)$ (expt.) (W.u.)	$B(M1)$ (SM) (W.u.)	$B(E2)$ (expt.) (W.u.)	$B(E2)$ (SM) (W.u.)
$3/2^+$	1431	$0, 1/2^+$	100	100	$-0.62(15)$	1.14	0.013(3)	0.0023	10(4)	6.1
$5/2^+$	1848	$0, 1/2^+$	93.6(9)	99.4	$-0.03(3)$				5.1(8)	5.6
		$1432, 3/2^+$	6.4(6)	0.6	0.09(18)	0.12	0.025(5)	0.0027	5^{+19}_{-5}	0.83

$B(E2; 3/2_1^+ \rightarrow 1/2^+) = 38.2\ e^2\,\mathrm{fm}^4$ (6.1 W.u.). The shell-model value of the mixing ratio is $|\delta| = 1.14$, whereas the experimental value is -0.62 ± 0.15 [42]. In the shell-model calculations, only the magnitude of the mixing ratio can be determined. In relation to the electromagnetic decay properties of the $3/2_1^+$ state of ^{33}P, the disagreement between experimental and shell-model lifetimes would appear to be related to the $M1$ component of the transition to the $1/2^+$ ground state. The experimental $M1$ transition rate (0.013 ± 0.003 W.u.) is in disagreement with that calculated in the present shell-model calculation, based on the PSDPF interaction; namely, 0.0023 W.u., as is the mixing ratio. Since the $M1$ transition is $\Delta\ell$ forbidden, it would seem likely that the transition proceeds through several smaller wave-function components in the initial and final states. In recent studies of the electromagnetic decay properties of states in ^{35}S [42] and ^{33}S [47], $B(M1; 3/2_1^+ \rightarrow 1/2_g^+)$ values were determined from previously measured lifetimes and compared with the results of shell-model calculations. For the $3/2_1^+ \rightarrow 1/2_g^+$ transition in ^{33}S, the shell-model calculations based on the USD and PSDPF interactions underestimate the experimental value by a factor of about two, whereas in ^{35}S the shell model based on the same interactions overestimates the measured value by a factor of about five.

D. Lifetime of second-excited $J^\pi = 5/2_1^+$ state of ^{33}P at 1848 keV

The $J^\pi = 5/2_1^+$ state of ^{33}P at 1848 keV decays to the ground state by an 1848-keV mixed $E2/M3$ transition and to the first-excited $3/2^+$ state at 1431 keV by a 417-keV mixed $M1/E2$ transition. The measured branching ratio, $I_\gamma(5/2_1^+ \rightarrow 3/2_1^+)/I_\gamma(5/2_1^+ \rightarrow 1/2^+)$, is 0.068 ± 0.006 [42]. In the present work, the 1848-keV transition was clearly observed in the γ-ray spectrum (see Fig. 2); however, the much weaker 417-keV γ-ray photopeak appears in a region of the spectrum dominated by peaks which correspond to the decay of target-like binary reaction products, the isotopes of Bi, and was consequently not observed. The 1848-keV state is fed by γ rays of energy 1643 and 2378 keV, which originate from the $J^\pi = 5/2_2^+$ state at 3491 keV and from the $J^\pi = 7/2_1^-$ state at 4226 keV, respectively. In the work of Hodsdon [17], which employed the same beam-target combination and the same beam energy, the measured relative intensities of the 1848-, 1643-, and 2378-keV γ-ray transitions were 100 ± 4, 16.0 ± 2.0, and 33.9 ± 2.4, respectively. Consideration therefore needs to be given to the effect of the feeding from these higher-lying states on the measured lifetime of the 1848-keV state. The lifetime of the $J^\pi = 5/2_2^+$ state has been measured as 0.09 ± 0.02 ps [44] and 0.11 ± 0.02 ps [45], while that of the $J^\pi = 7/2_1^-$ state has been measured to be 0.52 ± 0.10 ps [44] and 0.39 ± 0.10 ps [45]. The values adopted in a recent evaluation [42] are 84 ± 17 fs for the $5/2_2^+$ state and 0.46 ± 0.10 ps for the $7/2_1^-$ state. The lifetime of the $5/2_2^+$ state is too short to have any effect on the observed decay characteristics of the $5/2_1^+$ state. The $7/2_1^-$ state is fed by a $9/2_1^-$ state at 5451 keV with a measured lifetime of 35 ± 7 ps [48]. The relative intensity of the 1225-keV transition which feeds the $7/2_1^-$ state from the 5451-keV $J^\pi = 9/2_1^-$ state is, in relation to the intensities quoted earlier, 14.6 ± 2.1 units. Feeding from this state will therefore have an impact on the measured lifetime of the $5/2_1^+$ state.

To minimize the effects of feeding of the state of interest from higher-lying states, the $7/2_1^-$ state at 4228 keV in this particular case, and from the unobserved side-feeding transitions, an energy condition was applied to the PRISMA focal-plane Q value, generated from the measurement of ejectile energy. The robustness of the method was validated by reproducing known lifetimes in the present work and in lifetime measurements for the isotopes of sulfur from the same experimental data [28]. In particular, other than the good agreement between the present and adopted values of the lifetime of the first-excited 2^+ state of ^{34}P, discussed below, the measured lifetime of the $1/2^+$ state of ^{35}S at 1572 keV; namely 3.3(2) ps [28], is in excellent agreement with the adopted value of 3.3(5) ps [49]. Similarly, the measured lifetime of the 3^- state of ^{36}S at 4193 keV, 0.84(24) ps [28], is in very good agreement with the most recent published value of 0.9(1) ps [50]. This procedure will henceforth be referred to as corresponding to the application of a "Q gate." An example of a measured Q-value spectrum and its effect on the corresponding γ-ray spectrum will be given later, when the lifetime of the first 2^+ state of ^{34}P is being discussed.

Figure 5 shows a section of a γ-ray spectrum from 1800 to 2400 keV. The spectrum in blue corresponds to no Q gate while that in red corresponds to the application of a Q gate; it can be seen that the intensity of the 2378-keV photopeak is reduced in the gated spectrum in relation to that of the 1848-keV photopeak. Sections of a γ-ray spectrum for the 1848-keV transition corresponding to target-degrader distances of 7 and 120 μm are shown, with Gaussian fits to the two photopeaks, in Fig. 6. The statistics are poor; nevertheless, it can be seen that the ratios of the two components of the 1848-keV photopeak are very different at the two distances. As a result of the poor statistics, it is only possible to give a lifetime limit here, <2 ps, and this is consistent with the accepted value of 1.11 ± 0.16 ps [42].

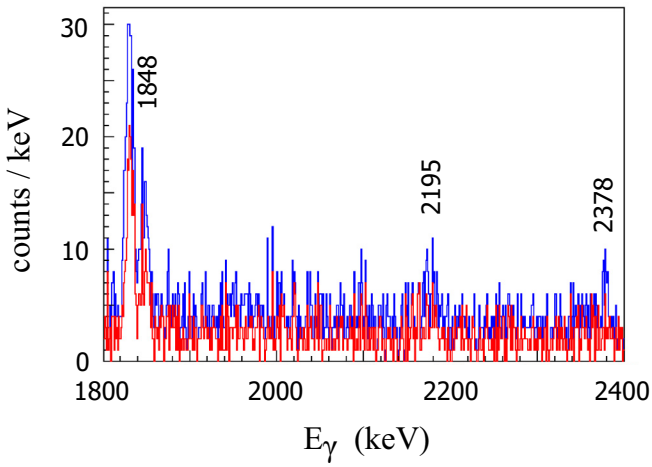

FIG. 5. Section of a ^{33}P γ-ray energy spectrum. The spectrum in blue corresponds to no Q gate while that in red corresponds to a Q gate ($Q> -35$ MeV) which results in the suppression of the 2378-keV γ-ray photopeak.

Shell-model calculations based on the PSDPF interaction [26] give the main component (24%) of the wave function of the $5/2^+_1$ state as

$$\pi(1d_{5/2})^5(2s_{1/2})^2 \otimes \nu(1d_{5/2})^6(2s_{1/2})^2(1d_{3/2})^2.$$

Table I presents a summary of the experimental and shell-model energies and lifetimes of the $5/2^+_1$ state. The level energy is well reproduced in the calculations. The lifetime limit from the present experiment and the previously adopted value from the 2011 evaluation of Chen *et al.* [42] are given. The shell-model lifetime (1.04 ps) is in very good agreement with the experimental value. There are other experimental electromagnetic decay properties of the state for which comparison can be made with the results of shell-model calculations. In Table II such a comparison is made for branching ratios, mixing ratios, and for $B(M1)$ and $B(E2)$ values. Experimental values were taken from the evaluation of Chen *et al.* [42]. The $5/2^+ \rightarrow 1/2^+$ transition is a mixed $E2/M3$ transition with a mixing ratio of $\delta = -0.03 \pm 0.03$ [42] [$\delta^2 = \lambda(M3)/\lambda(E2)$]; the decay is therefore dominated by $E2$ radiation, as expected. The $B(E2; 5/2^+_1 \rightarrow 1/2^+)$ value corresponding to the adopted lifetime is 5.1 ± 0.8 W.u. The corresponding shell-model value of 35.4 e^2 fm^4 (5.6 W.u.) is in excellent agreement with experiment. The branching ratio has been measured as $I_\gamma(5/2^+_1 \rightarrow 1/2^+) = 93.6\%$ and $I_\gamma(5/2^+_1 \rightarrow 3/2^+_1) = 6.4\%$ [42] and the corresponding values based on the results of shell-model calculations are 99.4% and 0.6%, which are not in good agreement with observation. The transition from the $5/2^+_1$ state at 1848 keV to the 1431-keV $J^\pi = 3/2^+_1$ state has an experimental mixing ratio [$\delta^2 = \lambda(E2)/\lambda(M1)$] of $\delta = 0.09 \pm 0.18$ [42] and the shell-model value is 0.12; the transition is therefore dominated by the $M1$ component. The large experimental uncertainty associated with the $B(E2; 5/2^+_1 \rightarrow 3/2^+_1)$ value makes a comparison with the shell model of very limited value. It would appear that the poor agreement with the measured branching ratio can be attributed to an underestimation of the magnitude of the $M1$ transition probability $B(M1; 5/2^+_1 \rightarrow 3/2^+_1)$ in the shell-model calculations; the shell-model value underestimates the measured value by a factor of about ten; see Table II. However, it should be noted, as in the case of the decay of the $3/2^+_1$ state, that the $B(M1)$ values where there is disagreement are very small. The good agreement of shell-model and experimental lifetimes is largely unaffected by the $M1$ transition rate from the $5/2^+_1$ state to the $3/2^+_1$ state, since the decay of the first $5/2^+$ state is dominated by the $5/2^+_1 \rightarrow 1/2^+$ $E2$ branch. For the $5/2^+_1 \rightarrow 3/2^+_1$ transition in ^{33}S [47], the shell-model (PSDPF interaction) underestimates the measured $B(M1)$ value by a factor of about three, whereas for the same transition in ^{35}S [51], the agreement between experiment and shell model is very good.

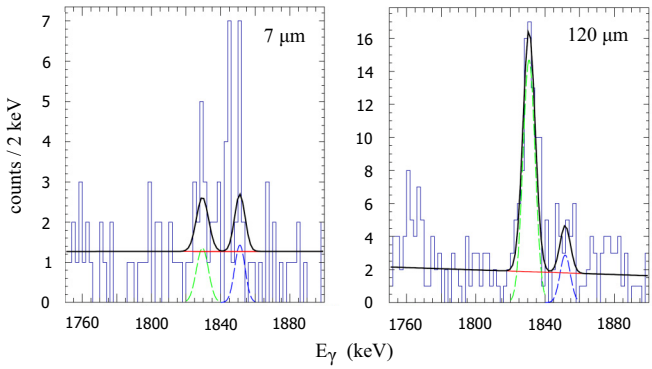

FIG. 6. Section of the measured γ-ray spectra for target-degrader distances of 7 and 120 μm corresponding to the 1848-keV $5/2^+$ to $1/2^+$ (ground-state) transition of ^{33}P. A Q gate has been applied to the γ-ray spectra (see text).

In an investigation of *sd*-shell observables for the USD, USDA, and USDB Hamiltonians, Richter *et al.* [37] noted that the two-body matrix elements (TBMEs) involving both $1d_{5/2}$ and $1d_{3/2}$ orbitals are relatively poorly determined by fits to energy data, because the 6–7 MeV single-particle energy splitting makes the contribution of these TBMEs to the energies of the low-lying states relatively small. The effect on the calculation of $M1$ transition rates in $5/2^+ \rightarrow 3/2^+$ transitions is particularly adversely affected because the matrix element of the $M1$ spin operator is large between $1d_{3/2}$ and $1d_{5/2}$ configurations. Throughout the present work, it will be seen, as for the above $M1$ transition rates in ^{33}P (Table II), that there are significant disagreements between experimental and shell-model values of $B(M1)$.

It is emphasized that the inclusion of the $3/2^+$ and $5/2^+$ states of ^{33}P in the present paper is justified mainly by the presentation of the first detailed shell-model analysis of the electromagnetic decay properties of the two states which has, in turn, resulted in the above significant conclusions.

E. Lifetimes in ^{34}P

The recent publication of Chapman *et al.* [9] summarizes the current experimental situation in relation to the study of the states of ^{34}P. The γ-ray spectrum measured in coincidence with ^{34}P ions is shown in Fig. 7. All of the labeled γ-ray peaks were previously identified in the earlier experiment [9,17].

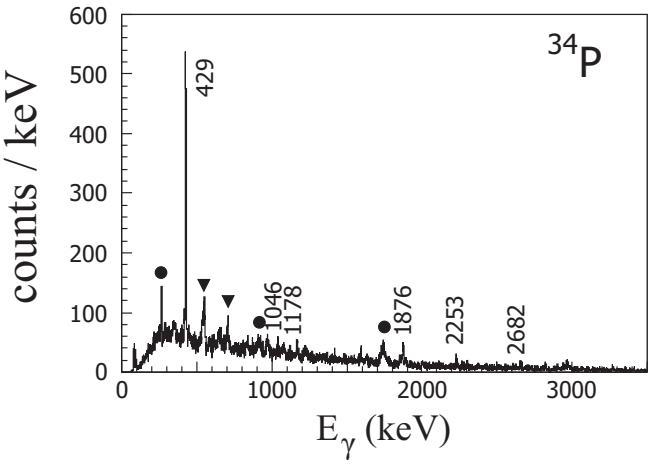

FIG. 7. γ-ray singles energy spectrum observed in coincidence with ^{34}P ions detected at the focal plane of PRISMA. The photopeaks labeled with ▼ and • correspond to γ-ray emission from the associated target-like fragments, ^{208}Bi and ^{209}Bi, respectively.

The level scheme based on the results of the earlier work is presented in Fig. 8. Here, the lifetime of the first-excited 2^+ state at 429 keV has been determined.

F. Lifetime of first-excited $J^\pi = 2^+$ state of ^{34}P at 429 keV

The photopeak at 429 keV dominates the γ-ray spectrum of Fig. 7. The lifetime of this state has most recently been measured to be $1.9^{+0.9}_{-0.5}$ ps [53]. The evaluation by Nica and Singh [52], which includes the recent value of Bender *et al.* [53], cites a lifetime value of $1.9^{+0.9}_{-0.4}$ ps. The 2^+ state is fed by the 1^+ state at 1607 keV, the 3^- state at 2320 keV, and the 4^- state at 2305 keV (via the 1178-, 1891-, and 1876-keV transitions, respectively), with γ-ray intensities relative to that

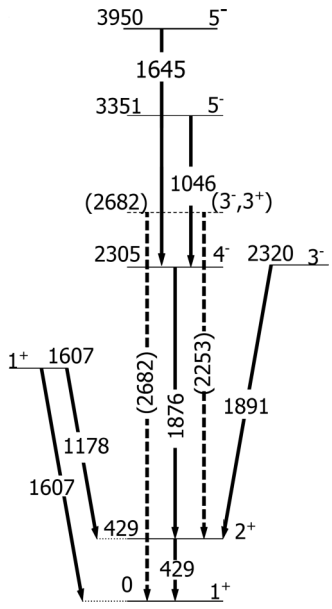

FIG. 8. Level scheme of ^{34}P from the earlier ^{36}S + ^{208}Pb experiment [9].

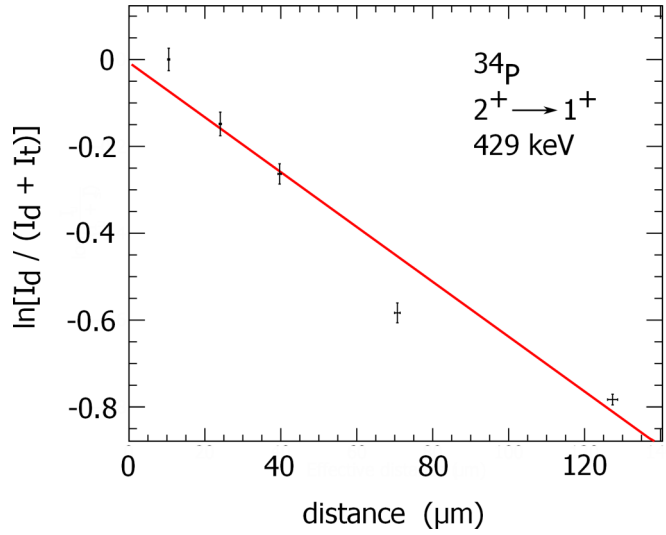

FIG. 9. The decay curve corresponding to the $2^+ \rightarrow 1^+$(ground-state) transition in ^{34}P with no correction for feeding of the state from higher-lying states. See text for details.

of the 429-keV transition, of $10.2 \pm 0.7\%$, $7.1 \pm 0.6\%$, and $24.4 \pm 0.9\%$, respectively [17]. The measured lifetimes of the feeding states have been measured as $0.75^{+0.65}_{-0.20}$ ps, >10 ps, and 2.90 ± 0.15 ns, respectively [53].

An analysis of the two components of the γ-ray photopeak corresponding to the 429-keV transition, without any correction being made for feeding from the higher-lying states, yields the decay curve of Fig. 9, with a corresponding lifetime of 1.8 ± 0.5 ps, in good agreement with the published value. In Fig. 9, I_t is the intensity of γ rays emitted from recoiling ^{34}P nuclei during their passage from target to degrader, while I_d is the intensity of γ rays emitted after the recoiling nuclei have passed through the degrader foil. In this, and in all subsequent decay curves presented here, the natural logarithm of the ratio $I_d/(I_d + I_t)$ is shown as a function of the target-to-degrader distance. A further analysis was performed in which a Q gate was applied to select the γ-ray photopeak of interest and remove both the feeding 1876- and 1891-keV transitions and also the unobserved side-feeding transitions. In the present work, the main contribution to the quoted uncertainties in the measured lifetimes comes from the statistical uncertainty in the number of counts in the γ-ray photopeaks.

Figure 10 shows γ-ray spectra corresponding to no Q gate (spectrum in blue) and with a Q gate (spectrum in red); the application of a Q gate greatly reduces the intensities of the 1876- and 1891-keV photopeaks. The figure also shows the gating condition which was applied to the PRISMA Q-value spectrum. Gaussian fits were then made to the two photopeak components corresponding to the 429-keV transition for each of the target-degrader distances. Figure 11 shows the two photopeak components for target-degrader distances of 7 and 120 μm, the shortest and longest distances. Finally, Fig. 12 presents the measured data together with the corresponding decay curve; a lifetime of 1.5 ± 0.5 ps has been obtained for the 2^+_1 state, which is in agreement, within the

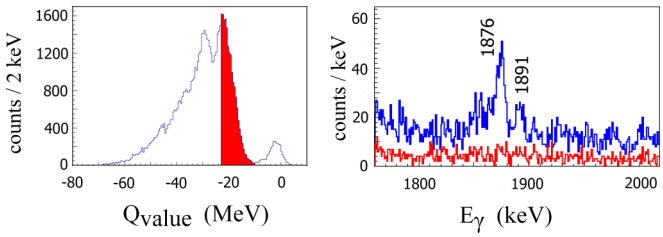

FIG. 10. (a) Q-value spectrum with the Q gate shown in red, and (b) a section of the measured γ-ray spectrum, which includes the 1876- and 1891-keV photopeaks, corresponding to no Q gate (spectrum in blue) and to a Q gate (spectrum in red). See text for details.

quoted experimental errors, with the value obtained with no Q gate applied, and in reasonably good agreement with the previously accepted value of $1.9^{+0.9}_{-0.4}$ ps.

In the context of the simple shell model, the ground state and first-excited state of ^{34}P are expected to result from the coupling of an unpaired $2s_{1/2}$ proton and a $1d_{3/2}$ neutron hole. The results of shell-model calculations performed using the $1\hbar\omega$ PSDPF interaction [26] show that this configuration represents 71% and 75% of the wave functions of the 1^+ and 2^+ states, respectively. Tables III and IV summarize the available experimental data in relation to the electromagnetic decay properties of the state. The shell-model excitation energy of 382 keV is in good agreement with the experimental value of 429 keV. The shell-model lifetime of 1.41 ps (Table III) is in very good agreement with the present measurement of 1.5(5) ps. The measured value of the $M1/E2$ mixing ratio for the 429-keV transition (Table IV) has a very large associated experimental uncertainty [52] and, consequently, comparison with the shell-model value of $\delta = 0.0024$ does not lead to any conclusion other than that the two values are consistent within experimental error. The consequent large experimental uncertainty in the $B(E2; 2^+ \rightarrow 1^+)$ value (Table IV) does not allow any meaningful conclusions to be made about the ability of the shell-model to reproduce the experimental value. The $2^+ \rightarrow 1^+$(ground-state) transition is essentially a pure $M1$ transition and, in contrast with the situation for ^{33}P, the shell model is able to reproduce the transition rate.

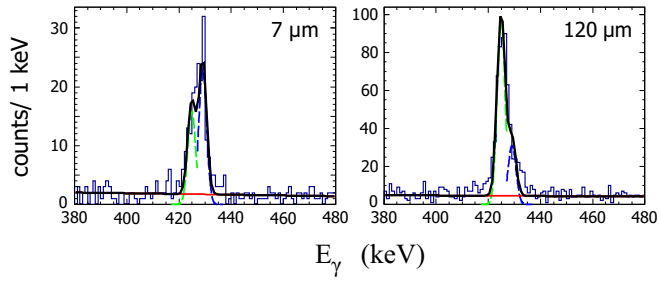

FIG. 11. Section of the measured γ-ray spectra for target-degrader distances of 7 and 120 μm corresponding to the 429-keV 2^+ to 1^+ (ground-state) transition in ^{34}P.

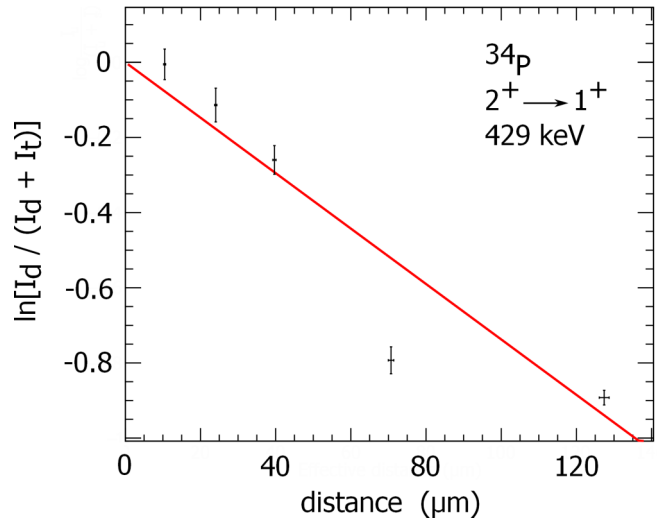

FIG. 12. The decay curve corresponding to the $2^+ \rightarrow 1^+$(ground-state) transition in ^{34}P with the removal of feeding through the application of a Q gate. See text for details.

G. Lifetimes in ^{35}P

The level structure of ^{35}P has been studied by a number of authors. The recent publication of Chapman *et al.* [9] summarizes the current experimental situation in relation to the study of the states of ^{35}P and their description within the context of $p - sd - pf$ shell-model calculations which used the PSDPF interaction [26]. The γ-ray spectrum measured in coincidence with ^{35}P ions is shown in Fig. 13. All of the labeled γ-ray peaks were previously identified in the earlier experiment carried out at INFN LNL [9,17]. The level scheme based on the results of the earlier experiment is presented in Fig. 14. In addition, the ^{35}P results of Ref. [9] have been revisited and, as a consequence, J^π values of $9/2^-$, $9/2^-$, and $11/2^-$ have been assigned to the states at excitation energies of 4766, 4962, and 5089 keV, respectively [54]. It is noted here that these are the J^π values suggested by Bouhelal *et al.* [55] in a shell-model description of phosphorus isotopes with $A = 30$–35. In the present work, lifetimes, or lifetime limits, have been established for the four states at 2386 keV with $J^\pi = 3/2^+_1$, at 3860 keV with $J^\pi = 5/2^+_1$, at 4101 keV with $J^\pi = 7/2^-_1$, and at 4493 keV with $J^\pi = 7/2^-_2$. No lifetimes of excited states of ^{35}P have previously been reported in the literature.

H. Lifetime of first-excited $J^\pi = 3/2^+_1$ state of ^{35}P at 2386 keV

The first-excited state of ^{35}P is fed by a 1474-keV transition from the higher-lying $J^\pi = 5/2^+_1$ state at 3860 keV. The

TABLE III. Experimental and shell-model values of excitation energy and lifetime of the 2^+_1 state of ^{34}P. The adopted lifetime is from Ref. [52].

J^π	E (expt.) (keV)	E (SM) (keV)	τ (present) (ps)	τ (adopted) (ps)	τ (SM) (ps)
2^+	429	382	1.5(5)	$1.9^{+0.9}_{-0.4}$	1.41

TABLE IV. Experimental and shell-model values of excitation energy and electromagnetic decay properties of the 2_1^+ state of ^{34}P. Experimental values are those from the Nuclear Data Sheets evaluation of Nica and Singh [52].

J^π	E (expt.) (keV)	E_f, J_f^π (keV)	δ (expt.)	$\lvert\delta\rvert$ (SM)	$B(M1)$ (expt.) (W.u.)	$B(M1)$ (SM) (W.u.)	$B(E2)$ (expt.) (W.u.)	$B(E2)$ (SM) (W.u.)
2^+	429	0, 1^+	$+0.11^{+0.13}_{-0.12}$	0.0024	$0.21^{+0.05}_{-0.10}$	0.28	50^{+130}_{-50}	0.035

intensity of the 1474-keV γ-ray transition in relation to that of the 2386-keV transition is $16.0 \pm 0.1\%$ [9,17]. The statistics for the 1474-keV γ-ray photopeak are poor; the stronger component of the peak in the energy spectrum corresponds to γ-ray emission before the recoiling nucleus reaches the degrader for all target-degrader distances, which implies that the effective lifetime of the state (which includes the effects of feeding from higher-lying states) is short. A Q gate was applied in order to reduce the effects of the feeding of the $3/2_1^+$ state from the $5/2_1^+$ state and the states which feed into the $5/2_1^+$ state. The effects of the unobserved side-feeding transitions were also minimized by this procedure. Figure 15 shows the two photopeak components in the γ-ray spectrum corresponding to the 2386-keV transition for target-degrader distances of 7, 65, and 120 μm. It can be concluded that the lifetime of the state is too short for a definitive measurement to be made here; consequently, a limit of <1 ps is estimated for the lifetime.

The shell-model wave function of the first $3/2^+$ state is dominated (91%) by the component

$$\pi(1d_{5/2})^6(2s_{1/2})^0(1d_{3/2})^1 \otimes \nu(1d_{5/2})^6(2s_{1/2})^2(1d_{3/2})^4,$$

whereas, for the ground-state, the component

$$\pi(1d_{5/2})^6(2s_{1/2})^1 \otimes \nu(1d_{5/2})^6(2s_{1/2})^2(1d_{3/2})^4$$

is the dominant one (90%). The electromagnetic transition between the two states therefore corresponds, to a very good approximation, to a proton making the transition from the $1d_{3/2}$ orbital to the $2s_{1/2}$ orbital and this is a mixed $M1/E2$ transition in which the $M1$ component is $\Delta\ell$ forbidden. Table V presents a summary of the experimental and shell-model energies and lifetimes for the states of interest here in ^{35}P. For the first $3/2^+$ state, the experimental level energy, 2386 keV, is well reproduced in the calculation (2553 keV) and the shell-model value of lifetime, 0.22 ps, is consistent with the present lifetime limit. Table VI presents the shell-model value of $M1/E2$ mixing ratio; unfortunately there is no published experimental value. The shell-model value of $B(M1; 3/2_1^+ \rightarrow 1/2^+) = 0.0089\mu_N^2$ (0.005 W.u.) is consistent with typical hindrance factors associated with $\Delta\ell$-forbidden $M1$ transitions [46]. The shell-model $B(E2; 3/2_1^+ \rightarrow 1/2^+)$ value is 24.6 e^2 fm^4 (3.61 W.u.).

I. Lifetime of second-excited $J^\pi = 5/2^+$ state of ^{35}P at 3860 keV

The 3860-keV photopeak in the spectrum of Fig. 13 corresponds to the transition from the $J^\pi = 5/2_1^+$ state at 3860 keV to the ground state. The photopeak corresponding to the 1474-keV branch (branching ratio $15 \pm 2\%$ [49]) can also be seen in the γ-ray spectrum; the intensity of the weaker branch is too small here for a lifetime measurement to be made. The 3860-keV state is fed directly from the states at 4101 keV and 4493 keV through transitions of energy 241 and 633 keV,

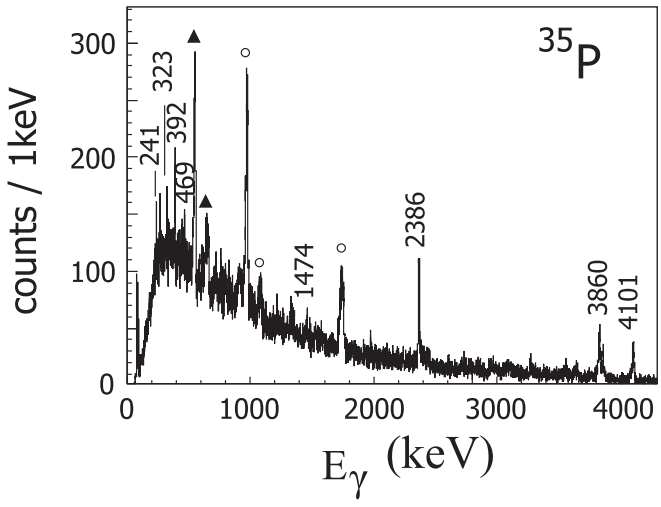

FIG. 13. γ-ray singles energy spectrum observed in coincidence with ^{35}P ions detected at the focal plane of PRISMA. Photopeaks labeled with the symbol ○ correspond to γ rays emitted from the associated target-like nucleus, ^{209}Bi, while those labeled with the symbol ▲ correspond to γ-ray emission from ^{208}Bi.

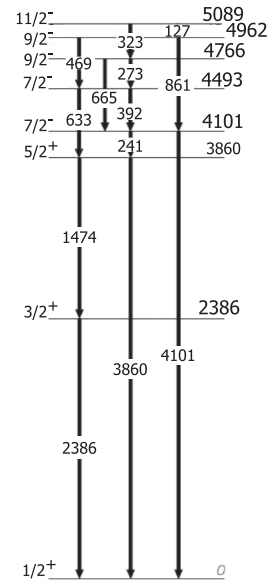

FIG. 14. Level scheme of ^{35}P observed in the earlier ^{36}S + ^{208}Pb experiment [9]. See text for details of the J^π values of the 4766-, 4962-, and 5089-keV states.

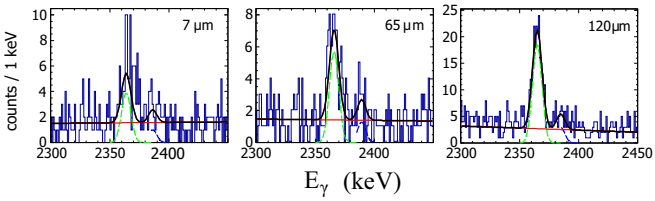

FIG. 15. Section of the measured γ-ray spectra for target-degrader distances of 7, 65, and 120 μm corresponding to the 2386-keV $3/2_1^+$ to $1/2^+$ (ground-state) transition of ^{35}P.

respectively. The intensities of the feeding transitions, relative to that of energy 3860 keV, have been measured as 32.6(4.3)% and 10.4(9.3)%, respectively [9,17]. In order to minimize the effects on the measured lifetime of feeding from these states and from the unobserved side-feeding states, a Q gate was applied. The resultant γ-ray spectrum, corresponding to all measured target-degrader distances, shows that the component of the 3860-keV photopeak corresponding to γ-ray emission occurring after the recoiling excited ^{35}P nucleus has passed through the degrader can no longer be observed; see Fig. 16. This implies that the lifetime of the 3860-keV state is short (<1 ps). In the ungated γ-ray spectrum of Fig. 13, it can be seen that both components are present, indicating that the higher-lying feeding states, both observed and unobserved, have an effective lifetime of a few ps.

The shell model predicts the first $5/2^+$ state to lie at 3976 keV, in good agreement with experiment (Table V). The predicted lifetime of the state, 29 fs, is also consistent with observation. The main component of the wave function (89%) of the $5/2_1^+$ state corresponds, as expected, to the proton-hole configuration

$$\pi(1d_{5/2})^5(2s_{1/2})^2(1d_{3/2})^0 \otimes \nu(1d_{5/2})^6(2s_{1/2})^2(1d_{3/2})^4.$$

Table VI presents the shell-model electromagnetic decay properties of the state. The electromagnetic transition to the ground state, a pure $E2$ transition, corresponds to a proton in the $2s_{1/2}$ orbital transferring to the $1d_{5/2}$ orbital. The $B(E2; 5/2_1^+ \rightarrow 1/2^+)$ value from the shell-model calculation is 27.9 $e^2\,\mathrm{fm}^4$ (4.10 W.u.). The $5/2_1^+$ state also decays by a mixed $M1/E2$ transition to the first-excited $3/2^+$ state at 2386 keV. There have been no experimental measurements of the mixing ratio reported in the literature. The very small shell-model mixing ratio, $|\delta| = 0.0052$, indicates that $M1$ electromagnetic decay dominates. The shell-model value of $B(E2; 5/2_1^+ \rightarrow 3/2_1^+)$, 0.013 $e^2\,\mathrm{fm}^4$ (1.91×10^{-3} W.u.), is thus very small. The $B(M1; 5/2_1^+ \rightarrow 3/2_1^+)$ value is $0.072\mu_N^2$ (4.00×10^{-2} W.u.). Finally, the shell-model branching ratio $I_\gamma(5/2_1^+ \rightarrow 3/2_1^+)/I_\gamma(5/2_1^+ \rightarrow 1/2^+)$ of 0.14 is in excellent agreement with observation, 0.15 ± 0.02 [49].

TABLE V. Experimental and shell-model values of excitation energies and lifetimes of states in ^{35}P.

J^π	E (expt.) (keV)	E (SM) (keV)	τ (present) (ps)	τ (SM) (ps)
$3/2_1^+$	2386	2553	<1	0.22
$5/2_1^+$	3860	3976	<1	0.029
$7/2_1^-$	4101	4185	>100	30
$7/2_2^-$	4493	4754	3.3(7)	4.87

J. Lifetime of $J^\pi = (7/2_1^-)$ state of ^{35}P at 4101 keV

The most recent compilation [49] gives the J^π value of the 4101-keV state of ^{35}P as $(7/2^-)$, the lowest-lying negative-parity state. The corresponding shell-model state is that at 4185 keV with $J^\pi = 7/2^-$. The dominant components of the wave function are

$$\pi(1d_{5/2})^6(2s_{1/2})^1(1d_{3/2})^0 \otimes \nu(1d_{5/2})^6(2s_{1/2})^2(1d_{3/2})^3(1f_{7/2})^1 \ (34\%)$$

and

$$\pi(1d_{5/2})^6(2s_{1/2})^0(1d_{3/2})^0(1f_{7/2})^1 \otimes \nu(1d_{5/2})^6(2s_{1/2})^2(1d_{3/2})^4 \ (21\%).$$

The second wave-function component above corresponds to the promotion of a proton in the ground state of ^{35}P from the $2s_{1/2}$ orbital to the $1f_{7/2}$ orbital, with an undisturbed neutron configuration; this corresponds to a simple shell-model picture of the $7/2^-$ state. However, there is also a significant wave-function component (34%) corresponding to the excitation of a neutron from the $1d_{3/2}$ orbital across the shell gap into the $1f_{7/2}$ orbital.

The photopeak at 4101 keV in the γ-ray spectrum of Fig. 13 corresponds to the ground-state decay of the 4101-keV state (52% branch) [56]. The state also decays to the 3860-keV $J^\pi = 5/2_1^+$ state by the emission of a 241-keV γ ray (39% branch) and to the 2386-keV $J^\pi = 3/2_1^+$ state (9% branch) through the emission of a 1714.8-keV γ ray. The photopeak corresponding to the latter transition is not observed here. The "shifted" component in the photopeak corresponding to the 4101-keV transition (γ-ray emission before the excited ^{35}P nucleus has passed through the degrader) is very weak, which implies that the effective lifetime is long; see Fig. 17. The 4101-keV state is populated directly from higher-lying states of energy 4493 ($J^\pi = 7/2_2^-$), 4766 ($J^\pi = 9/2_1^-$), and 4962 keV ($J^\pi = 9/2_2^-$); the corresponding γ-ray transitions of energy 392, 665, and 861 keV have intensities, relative to that of the 4101-keV transition, of 72(11)%, 51(11)%, and 28(15)% [9,17]. The long lifetime does not appear to be associated with feeding from higher-lying states. The 861-keV, $(9/2_2^-) \rightarrow (7/2_1^-)$, γ-ray photopeak is not observed in the spectrum of Fig. 13. Note that the shell-model lifetime of the $9/2_2^-$ state is 5.5 ps. The photopeak corresponding to the 665-keV $(9/2_1^-) \rightarrow (7/2_1^-)$ transition has two components, which implies that the effective lifetime is of the order of a few ps; the shell-model value of lifetime is 0.13 ps. Finally, the lifetime of the $(7/2_2^-)$ state at 4493 keV, which feeds the 4101-keV state through a 392-keV transition, has a measured lifetime, in the present work, of 3.3(7) ps, which is short compared with the lifetime of the $7/2_1^-$ state. It can therefore be concluded that the measured long lifetime of the $(7/2_1^-)$ state is not associated with its feeding from higher-lying states, although this conclusion is to some extent model dependent.

TABLE VI. Experimental and shell-model values of electromagnetic decay properties of states in ^{35}P. Experimental values of branching ratio are those from Refs. [49], [56], and [9] for the $5/2_1^+$, $7/2_1^-$, and $7/2_2^-$ states, respectively. See text for details.

J^π	E (expt.) (keV)	E_f, J_f^π (keV)	BR (expt.) (%)	BR (SM) (%)	$\|\delta\|$ (SM)	$M\lambda$, $B(M\lambda)$ (SM) (W.u.)	$E\lambda$, $B(E\lambda)$ (SM) (W.u.)
$3/2_1^+$	2386	0, $1/2^+$	100	100	1.05	$M1$, 0.005	$E2$, 3.61
$5/2_1^+$	3860	0, $1/2^+$	87	88			$E2$, 4.10
		2386, $3/2^+$	13(2)	12	0.0052	$M1$, 0.040	$E2$, 0.0019
$7/2_1^-$	4101	0, $1/2^+$	52(4)	27			$E3$, 10.5
		2386, $3/2^+$	9(2)	16	0.031	$M2$, 1.41	$E3$, 2.61
		3860, $5/2^+$	39(2)	57			$E1$, 0.0012
$7/2_2^-$	4493	3860, $5/2^+$	15(3)	73			$E1$, 0.00054
		4101, $7/2^-$	85(4)	27	0.0067	$M1$, 0.028	$E2$, 0.032

Figure 18 shows the photopeak corresponding to the 4101-keV transition for three of the five measured target-degrader distances. It can be seen that the component corresponding to γ-ray emission after the degrader is the only component observed. It can therefore be concluded that the lifetime of the $(7/2_1^-)$ state is greater than about 100 ps.

Of the two main wave-function components given above for the $7/2_1^-$ state, the second, with an admixture of 21%, is expected to play a significant role in the electromagnetic decay process to the ground state; when this particular component is involved in the γ-ray emission process, the $E3$ transition corresponds to the unpaired proton making the $\Delta j = \Delta\ell = 3$ transition $\pi(1f_{7/2}) \rightarrow \pi(2s_{1/2})$. The shell-model value of the lifetime is 30 ps, which is not inconsistent with the long-lifetime limit associated with the experimental measurement here; see Table V. The first $7/2^-$ state decays to the $1/2^+$ ground state by an $E3$ transition, to the first $3/2^+$ state at 2386 keV by a mixed $M2/E3$ transition, and to the first $5/2^+$ state at 3860 keV by an $E1$ transition. Table VI presents the shell-model electromagnetic decay properties of the state. The shell-model values of branching ratios, 57%, 16%, and 27% to the $5/2_1^+$, $3/2_1^+$, and $1/2_1^+$ states, respectively, are not in good agreement with the corresponding measured values of 39(2)%, 9(2)%, and 52 (4)% [56]. It is noted that the experimental branching ratios of the first $7/2^-$ state, given in the Nuclear Data Sheets evaluation [49], are not in agreement with those of Dufour *et al.* [56] and of Chapman *et al.* [9,17], which are consistent within experimental errors. Consequently, in Table VI, the quoted values are those of Dufour *et al.* [56]. Reduced electromagnetic transition rates predicted by the shell model are $B(E3; 7/2_1^- \rightarrow 1/2_1^+) = 761\ e^2\,\mathrm{fm}^6$ (10.5 W.u.), $B(E3; 7/2_1^- \rightarrow 3/2_1^+) = 190\ e^2\,\mathrm{fm}^6$ (2.61 W.u.), $B(M2; 7/2_1^- \rightarrow 3/2_1^+) = 25.0\mu_N^2\,\mathrm{fm}^2$ (1.41 W.u.), and $B(E1; 7/2_1^- \rightarrow 5/2_1^+) = 0.00081\ e^2\,\mathrm{fm}^2$ (1.2×10^{-3} W.u.). For the $7/2_1^- \rightarrow 1/2_1^+$ transition, the shell-model value of the $E3$ transition rate (10.5 W.u.) is large, as expected for a $\Delta j = \Delta\ell = 3$ transition.

K. Lifetime of $J^\pi = (7/2_2^-)$ state of ^{35}P at 4493 keV

The J^π value of the 4493-keV state is given as $(7/2^-)$ in the latest evaluation of $A = 35$ isotopes [49]. The state decays to the $J^\pi = (7/2_1^-)$ state at 4101 keV by the emission of a

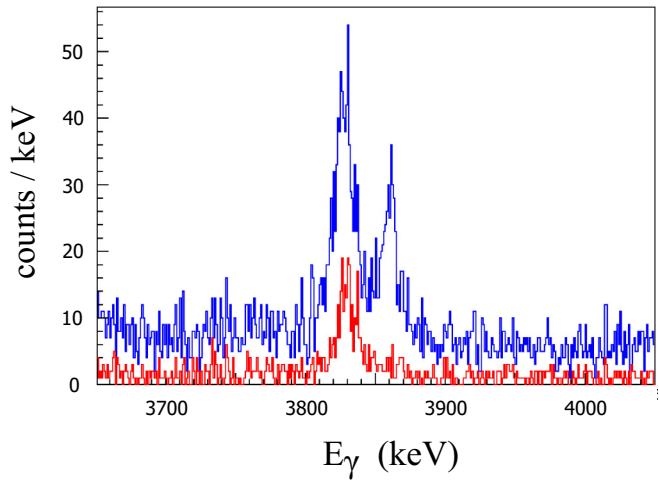

FIG. 16. Sections of γ-ray spectra which show the two components of the 3860-keV γ-ray photopeak with a Q gate ($Q > -17$ MeV) (spectrum in red) and without a gate (in blue). See text for details.

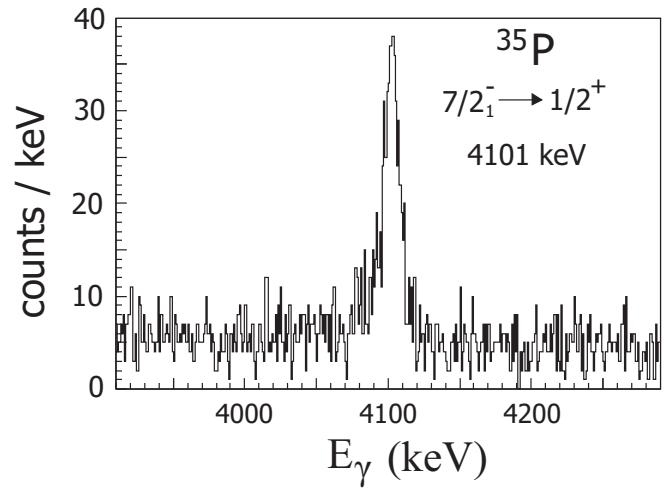

FIG. 17. Section of a γ-ray spectrum which show the 4101-keV γ-ray photopeak. The spectrum corresponds to the sum of γ-ray spectra at all five target-degrader distances. See text for details.

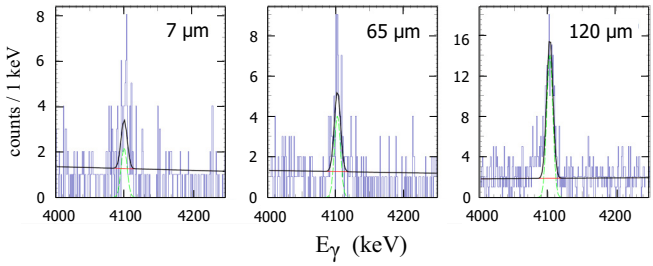

FIG. 18. Section of the measured γ-ray spectra for target-degrader distances of 7, 65, and 120 μm corresponding to the 4101-keV $(7/2_1^-) \rightarrow 1/2^+$ (ground-state) transition of ^{35}P.

392-keV γ ray; the corresponding photopeak is observed in the spectrum of Fig. 13. The γ-ray photopeak corresponding to the 633.7-keV branch to the 3860-keV state (15%) [49] is not observed in the present work as a consequence of its low intensity and the nearby presence of broad target-like photopeak structures. The 4493-keV state is fed directly from above by the $9/2_1^-$ state at 4766 keV and by the $9/2_2^-$ state at 4962 keV. The intensities of the corresponding transitions, at 273 and 469 keV, relative to the 392-keV transition, are 52(4)% and 67(5)%, respectively [9,17]. The statistics in the present experiment for the corresponding photopeaks are poor; nevertheless, a Q gate was applied in order to reduce the effects of the feeding transitions, both observed and unobserved. Figure 19 shows the effect of the application of a Q gate on the γ-ray spectrum; the intensities of the 273- and 469-keV feeding transitions are reduced in the gated spectrum, although it has not been possible to remove the 469-keV peak completely. In shell-model calculations based on the PSDPF interaction, the lifetime of the $9/2_1^-$ state is short; namely, 0.13 ps, and, on this basis, the contribution to the measured lifetime of the $7/2_2^-$ state can be neglected. As noted earlier, the shell-model lifetime of the $9/2_2^-$ state is 5.5 ps. The two components of the 392-keV γ-ray photopeak,

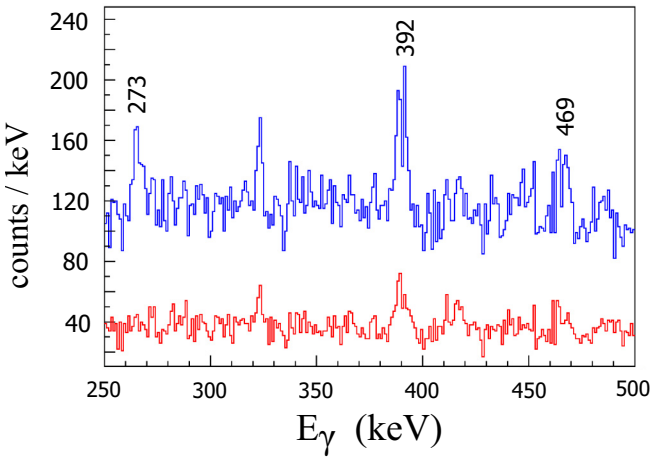

FIG. 19. Sections of γ-ray spectra which show the two components of the 392-keV γ-ray photopeak and the feeding transitions at 273 and 469 keV with (spectrum in red) a Q gate and (in blue) without a Q gate. See text for details.

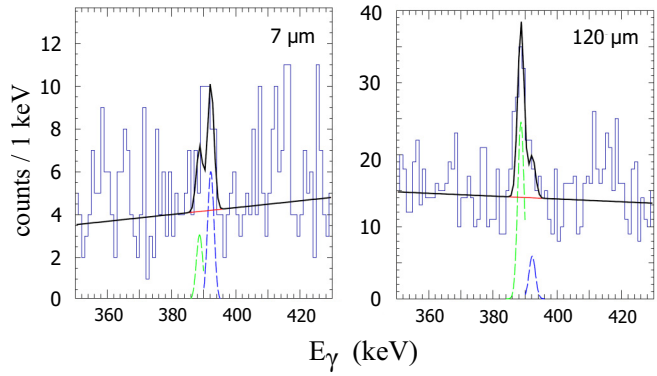

FIG. 20. Sections of the measured γ-ray spectra for target-degrader distances of 7 and 120 μm corresponding to the 392-keV $(7/2_2^-)$ to $(7/2_1^-)$ transition of ^{35}P.

together with Gaussian fits, corresponding to target-degrader distances of 7 and 120 μm are shown in Fig. 20. Figure 21 presents the corresponding decay curve. The measured lifetime is 3.3 ± 0.7 ps.

p-sd-pf shell-model calculations based on the PSDPF residual interaction predict that the second $7/2^-$ state lies at an excitation energy of 4754 keV, about 260 keV higher in energy than the observed state; see Table V. The wave function has, as its main component (49%), the configuration

$$\pi(1d_{5/2})^6(2s_{1/2})^1 \otimes \nu(1d_{5/2})^6(2s_{1/2})^2(1d_{3/2})^3(1f_{7/2})^1,$$

which corresponds to the promotion of a neutron across the $N = 20$ shell gap from the $1d_{3/2}$ orbital in the ^{35}P ground state to the $1f_{7/2}$ orbital. The shell-model value of lifetime, 4.87 ps, is in good agreement with the result of the present measurement; namely, 3.3 ± 0.7 ps; see Table V. The $(7/2_2^-)$ state decays to the $5/2_1^+$ state at 3860 keV by an $E1$ transition and to the $7/2_1^-$ state by a mixed $M1/E2$ transition. The experimental and shell-model branching ratios (see Table VI)

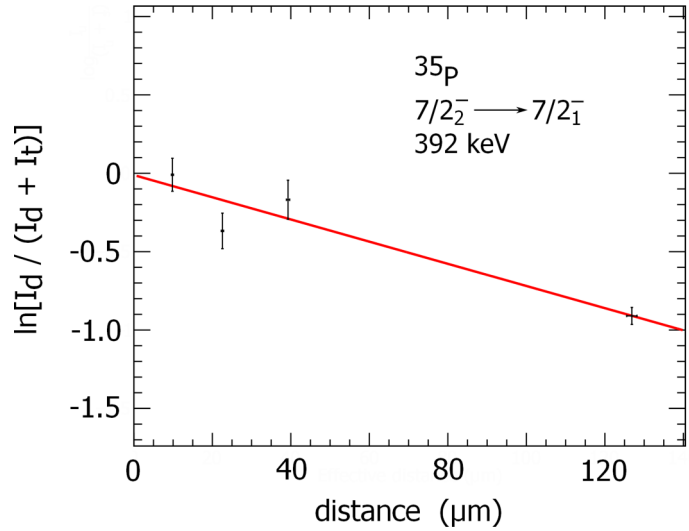

FIG. 21. The decay curve corresponding to the $(7/2_2^-) \rightarrow (7/2_1^-)$ transition in ^{35}P.

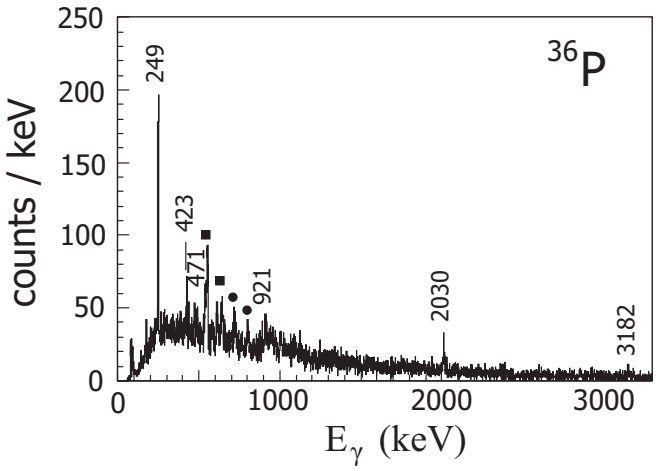

FIG. 22. γ-ray singles energy spectrum observed in coincidence with ^{36}P ions detected at the focal plane of PRISMA. Photopeaks labeled with the symbol • correspond to γ-ray emission from ^{207}Bi, while those labeled with the symbol ■ correspond to emission from ^{208}Bi.

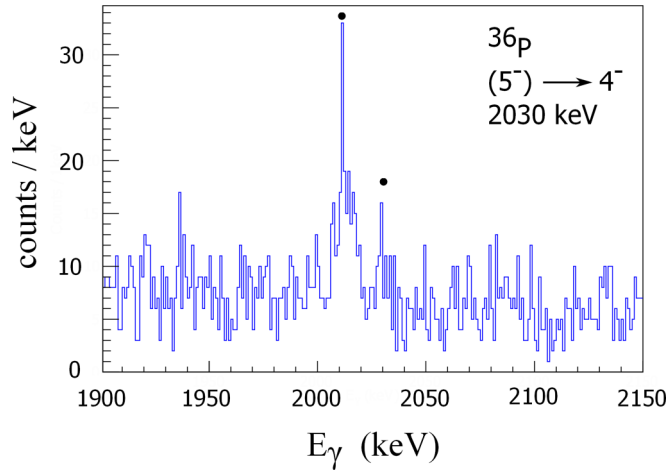

FIG. 24. Section of the measured ^{36}P γ-ray spectrum which shows the two components of the 2030-keV photopeak, labeled with the symbol •, and corresponding to the (5^-) to 4^- transition. Spectra at all measured target-degrader distances have been summed to produce the γ-ray spectrum.

are in very poor agreement. The values of branching ratio given in the evaluation of Chen *et al.* [49], which are based on the work of Wiedeking *et al.* [57] (private communication),

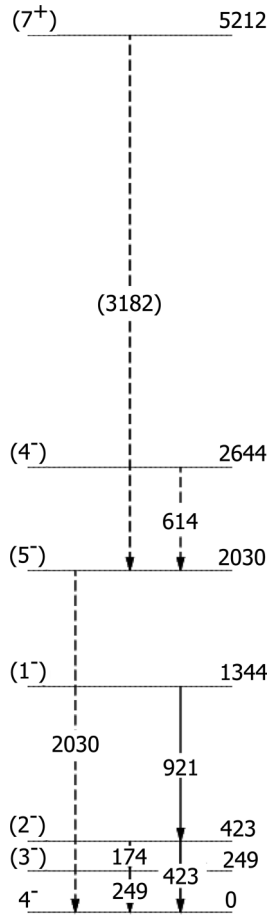

FIG. 23. Level scheme of ^{36}P observed in the earlier ^{36}S + ^{208}Pb experiment [9,17].

are not in agreement with those of Dufour *et al.* [56] and of Chapman *et al.* [9]. Consequently, in Table VI the values which are quoted are those of Chapman *et al.* [9], which are in excellent agreement with the values of Dufour *et al.* The three independent measurements of branching ratio agree that the decay to the $7/2^-_1$ state is much stronger than to the $5/2^+_1$ state. Why the shell model is unable to reproduce the decay characteristics of the state is not understood at the present time. The very small value of shell-model mixing ratio for the transition $7/2^-_2 \rightarrow 7/2^-_1$, $|\delta| = 0.0067$, implies that this decay branch is dominated by $M1$ radiation. Thus, how the $7/2^-_2$ decays to the lower lying $7/2^-_1$ and $5/2^+_1$ states is determined by the strengths of the competing $M1$ and $E1$ radiation, and here the results from the shell model are in stark disagreement with observation. This would appear to be consistent with earlier conclusions here with reference to shell-model values of $B(M1)$ being underestimated. It is also noted here that shell-model values of $B(E1)$ using the PSDPF interaction are too small compared with experimental values [58]. Reduced electromagnetic transition probabilities calculated using the shell model (see Table VI) are $B(E1; 7/2^-_2 \rightarrow 5/2^+_1) = 0.00037\ e^2\,\mathrm{fm}^2$ $(5.4 \times 10^{-4}$ W.u.), $B(M1; 7/2^-_2 \rightarrow 7/2^-_1) = 0.051\mu_N^2$ $(2.8 \times 10^{-2}$ W.u.), and $B(E2; 7/2^-_2 \rightarrow 7/2^-_1) = 0.21\ e^2\,\mathrm{fm}^4$ $(3.2 \times 10^{-2}$ W.u.). Although there is

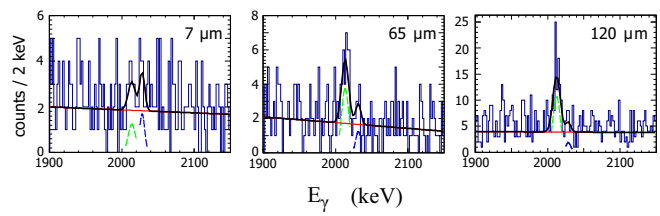

FIG. 25. Section of the measured γ-ray spectra for target-degrader distances of 7, 65, and 120 μm corresponding to the 2030-keV (5^-) to 4^- transition of ^{36}P.

TABLE VII. Experimental and shell-model values of excitation energies and lifetimes of states in ^{36}P.

J^π	E (expt.) (keV)	E (SM) (keV)	τ (present) (ps)	τ (SM) (ps)
(5^-)	2030	1817	<1	0.29
(7^+)	5212		2.7(6)	

good agreement between experiment and the shell model for the excitation energy and lifetime, the disagreement with branching ratios might indicate that there has been an incorrect association of experimental and shell-model states. The J^π value of the 4493-keV state is tentative; a definitive measurement would be helpful.

L. Lifetimes in ^{36}P

The recent publication of Chapman *et al.* [9] summarizes the current experimental situation in relation to the study of the states of ^{36}P. The γ-ray spectrum measured in coincidence with ^{36}P ions is shown in Fig. 22. The statistics are quite poor. All of the labeled γ-ray peaks were previously identified in the earlier experiment [9,17]. The level scheme based on the results of that experiment is presented in Fig. 23. In the present work, the lifetimes of the (5^-) level at 2030 keV and that at 5212 keV with $J^\pi = (7^+)$ have been measured. Unfortunately, it has not been possible to measure the lifetimes of the low-lying states; however, a discussion of the shell-model electromagnetic decay properties of the (3^-) and (1^-) states will be included here for completeness.

M. Lifetime of $J^\pi = (5_1^-)$ state of ^{36}P at 2030 keV

The proposed $J^\pi = (5^-)$ state at 2030 keV has recently been discussed by Chapman *et al.* [9]. The stretched state is one in which, in this case, a $1d_{3/2}$ proton is coupled to the odd-neutron in the $1f_{7/2}$ orbital. The shell-model counterpart of the state, based on the PSDPF interaction, is at 1817 keV with the above component accounting for 79% of the total wave function [9]. The 2030-keV photopeak, corresponding to decay of the state to the ground state, may be seen in the γ-ray spectrum of Fig. 22. That the observed decay of the state, which includes the effect of feeding from the higher-lying (7^+) and (4^-) states, lies in the appropriate range for measurement in the present experiment is demonstrated in the spectrum of Fig. 24; both photopeak components are observed although, again, the statistics are poor. Figure 25 shows Gaussian fits to the two components of the 2030-keV photopeak corresponding to target-degrader distances of 7, 65, and 120 μm and Fig. 26 presents the decay curve. It can be concluded that the lifetime of the (5^-) state is no larger than 1.6 ± 0.9 ps. Because of the poor statistics, it is difficult to satisfactorily apply a Q gate in order to remove the effects of the feeding of the (5^-) state by the (7^+) and (4^-) states and by direct side feeding from unobserved transitions. The intensity of the 3182-keV transition $[(7^+) \rightarrow (5^-)]$ is 51(5)% of that of the 2030-keV transition, while that of the 614-keV transition $[(4^-) \rightarrow (5^-)]$ is 34(4)% [9,17]. When a Q gate is applied, the two components of the 2030-keV photopeak are visible only for the shortest three target-to-degrader distances; at the two longest distances of 65 and 120 μm, only the Doppler-shifted component is present. This observation leads to an estimated state lifetime of <1 ps.

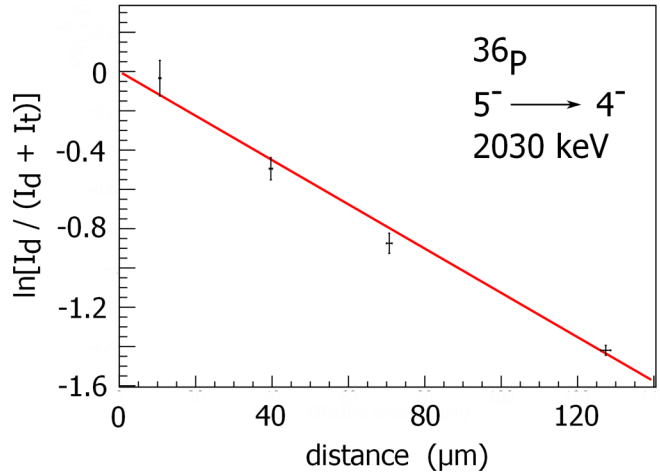

FIG. 26. The decay curve corresponding to the $(5^-) \rightarrow 4^-$ transition in ^{36}P.

Tables VII and VIII summarize the experimental and shell-model decay properties of the first 5^- state. The decay to the 4^- ground state is of mixed $M1/E2$ multipolarity, while decay to the first 3^- state is through the emission of $E2$ radiation. The shell-model lifetime of the 5^- state is 0.29 ps (Table VII), which is consistent with the experimental limit based on the current work. For the 2030-keV transition, the shell-model value of the mixing ratio is 0.24; see Table VIII. The shell-model values of $B(M1; 5^- \rightarrow 4^-)$ and of $B(E2; 5^- \rightarrow 4^-)$ are also given in the table. For the hitherto unobserved 1781-keV $5^- \rightarrow 3^-$ transition, the $B(E2)$ value is calculated to be 23.7 e^2 fm^4 (3.35 W.u.) and the branching of the state, $I_\gamma(5^- \rightarrow 4^-) = 85\%$, is consistent with the nonobservation of the $5^- \rightarrow 3^-$ transition in previous experimental work [9].

TABLE VIII. Experimental and shell-model values of electromagnetic decay properties of states in ^{36}P.

J^π	E (expt.) (keV)	E_f, J_f^π (keV)	BR (expt.) (%)	BR (SM) (%)	δ (expt.)	$\lvert\delta\rvert$ (SM)	$B(M1)$ (expt.) (W.u.)	$B(M1)$ (SM) (W.u.)	$B(E2)$ (expt.) (W.u.)	$B(E2)$ (SM) (W.u.)
3^-	249	$0, 4^-$	100	100		0.0023		0.87		0.26
5^-	2030	$0, 4^-$	100	85		0.24		0.010		0.51
		$249, 3^-$	0	15						3.35
7^+	5212	$2030, (5^-)$								

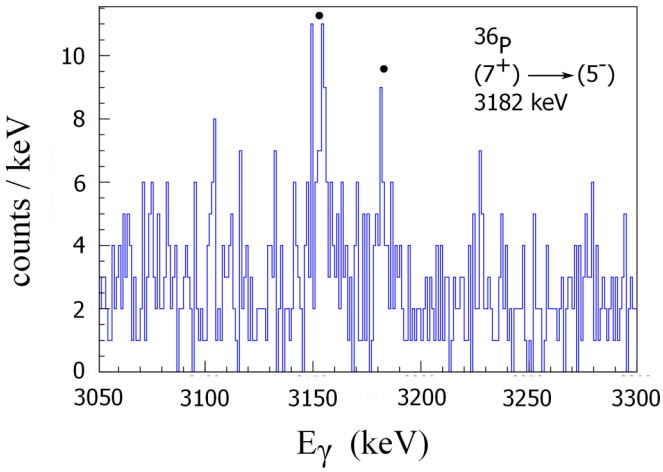

FIG. 27. Section of the measured ^{36}P γ-ray spectrum which shows the two components of the 3182-keV (7^+) to (5^-_1) transition, indicated with the symbol •. Spectra at all measured target-degrader distances have been summed to produce the γ-ray spectrum.

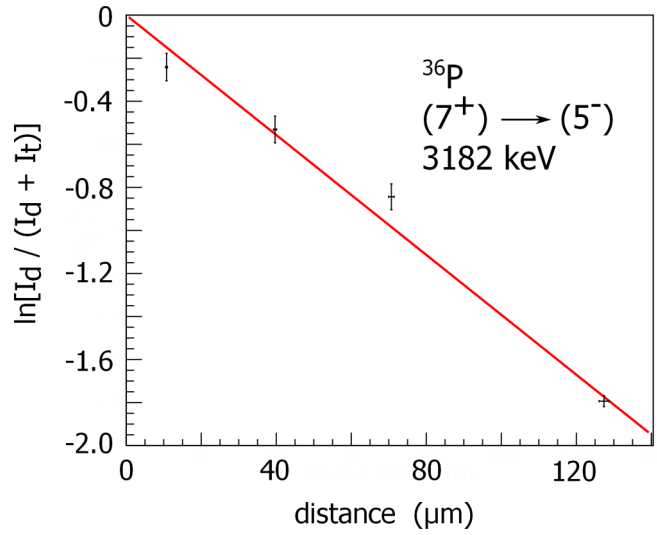

FIG. 29. The decay curve corresponding to the $(7^+) \rightarrow (5^-)$ transition in ^{36}P.

N. Lifetime of $J^\pi = (7^+)$ state of ^{36}P at 5212 keV

The weak photopeak at 3182 keV in the spectrum of Fig. 22 corresponds to the transition from the $J^\pi = (7^+)$ state to the 2030-keV state with $J^\pi = (5^-)$. The state has earlier been discussed in terms of the stretch configuration $\nu(1f_{7/2}) \otimes \pi(1f_{7/2})$ [9]. Such states have been observed in the even-A isotopes of phosphorus with $A = 30$, 32, 34, and 36 and, for these states, the np separation energy $S(np)$ shows a linear relationship with mass number [59], an effect first discussed within the context of the Bansal-French [60] model. While the statistics for the 3182-keV photopeak in the present experiment are poor, an attempt has nevertheless been made to extract a lifetime for the (7^+) state. Since there is no observed feeding from higher-lying states, the lifetime has been extracted by using the measured intensities of the two components of the 3182-keV photopeak at the various target-degrader distances. Figure 27 shows the two components of the 3182-keV photopeak using the full statistics of the experiment, i.e., a spectrum corresponding to all measured target-degrader distances. Although the statistics are poor, it is clear that there are two components to the photopeak, corresponding to decay before and after passage of recoiling excited ^{36}P nuclei through the degrader foil. Figure 28 shows the two components of the 3182-keV photopeak for target-degrader distances of 7, 65, and 120 μm and the corresponding decay curve is shown in Fig. 29. The measured lifetime is $\tau = 2.7 \pm 0.6$ ps. The shell model, based on the PSDPF interaction is not able to calculate the properties of the 7^+ state, since its wave function involves the occupation of the $1f_{7/2}$ shell-model state by one proton and one neutron and this lies outside the configuration space of the model.

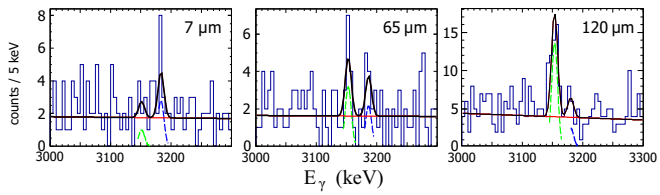

FIG. 28. Sections of the measured γ-ray spectra for target-degrader distances of 7, 65, and 120 μm corresponding to the 3182-keV (7^+) to (5^-_1) transition of ^{36}P.

O. The first-excited $J^\pi = (3^-)$ and (1^-) states of ^{36}P

The first-excited state of ^{36}P at an excitation energy of 249 keV has been tentatively assigned a J^π value of (3^-) [9]. The shell model predicts a first-excited state at 238 keV with a J^π value of 3^- and lifetime 2.3 ps. Table VIII summarizes the shell-model decay properties of the 3^- state. Electromagnetic decay to the 4^- ground state takes place via a mixed $M1/E2$ transition. The shell-model value of $M1$ transition strength, $B(M1; 3^- \rightarrow 4^-) = 1.56\mu_N^2$ (0.87 W.u.), is very strong; see Table VIII. The first 3^- and 4^- (ground) states correspond to the two possible couplings of the unpaired $2s_{1/2}$ proton and the unpaired $1f_{7/2}$ neutron. These configurations contribute 70% and 75% to the total shell-model wave functions of the 3^- and 4^- states, respectively [9]. The $M1$ transition is therefore essentially a pure spin-flip transition, which accounts for the large $M1$ transition strength. It would be very interesting to confirm the large strength experimentally.

Coupling of an odd $2s_{1/2}$ proton with the unpaired $2p_{3/2}$ neutron leads to states with J^π values of 1^- and 2^- at predicted excitation energies of 1552 and 282 keV with contributions of 75% and 56%, respectively, to the total wave function of the states. The proposed experimental counterparts are at excitation energies of 1344 and 423 keV, respectively [9]. The shell-model value of $B(M1; 1^- \rightarrow 2^-)$; namely, $1.41\mu_N^2$ (0.79 W.u.), corresponding once again to a spin-flip transition, is very large. The electromagnetic decay properties of the two states have been discussed here for completeness, and especially since the predicted $M1$ transition rates are high.

IV. CONCLUSIONS

Lifetimes of excited states of the phosphorus isotopes ^{33,34,35,36}P, populated in binary grazing reactions, were measured using the differential recoil-distance method. The statistics of the γ-ray spectra corresponding to the different target-to-degrader distances are poor; nevertheless, a few lifetime measurements and lifetime limits have been determined. The resulting lifetimes are in good agreement with earlier measurements, where available, which confirms the robustness of the present measurements. For ^{35}P and ^{36}P, there are no previous published lifetime values. Lifetimes, mixing ratios, where available from published work, branching ratios, and electromagnetic transition rates have been compared with the results of shell-model calculations based on the PSDPF effective interaction. In general, there is good agreement between experiment and shell model. However, there is evidence that shell-model values of $M1$ transition rates for the $3/2^+_1 \rightarrow 1/2^+_1$ (ground state) and $5/2^+_1 \rightarrow 3/2^+_1$ transitions in ^{33}P underestimate the experimental values by a factor of between 5 and 10. The two-body matrix elements which involve both $1d_{5/2}$ and $1d_{3/2}$ orbitals are relatively poorly defined in the USDB interaction and this may contribute to the observed differences between experiment and the shell model in this case. In ^{35}P, there is poor agreement between experiment and the shell model for the branching ratio of the $7/2^-_2$ state at an experimental excitation energy of 4493 keV; in this case, the competing electromagnetic decay branches are dominated by $E1$ and $M1$ transitions. The reasons for this discrepancy are not understood at the present time. Further measurements of electromagnetic decay properties in this region of the nuclear chart would be helpful in refining the shell-model effective interactions.

ACKNOWLEDGMENTS

The authors would like to thank the members of the AGATA collaboration for the design and development of the AGATA γ-ray tracking array used in the present experiment. The work of the team at The Institute für Kernphysik der Universitat zu Köln which developed the recoil-distance differential plunger apparatus is also gratefully acknowledged. This work was supported by the UK Science and Technologies Facility Council (STFC) under Grants No. ST/L005808/1 (UWS) and No. ST/P005101/1 (UWS). T.M. and S.S. acknowledge support in part from the Croatian Science Foundation under Project No. 7194. Finally, the contribution of the accelerator and target-fabrication staff at the INFN Legnaro National Laboratory is gratefully acknowledged.

[1] A. Dewald, S. Harissopulos, and P. von Brentano, Z. Phys. A **334**, 163 (1989).
[2] A. Dewald, O. Möller, and P. Petkov, Prog. Part. Nucl. Phys. **67**, 786 (2012).
[3] J. J. Valiente-Dobon, D. Mengoni, A. Gadea, E. Farnea, S. M. Lenzi, S. Lunardi, A. Dewald, Th. Pissulla, S. Szilner, R. Broda, F. Recchia, A. Algora, L. Angus, D. Bazzacco, G. Benzoni, P. G. Bizzeti, A. M. Bizzeti-Sona, P. Boutachkov, L. Corradi, F. Crespi, G. de Angelis, E. Fioretto, A. Görgen, M. Gorska, A. Gottardo, E. Grodner, B. Guiot, A. Howard, W. Królas, S. Leoni, P. Mason, R. Menegazzo, D. Montanari, G. Montagnoli, D. R. Napoli, A. Obertelli, T. Pawlat, G. Pollarolo, B. Rubio, E. Sahin, F. Scarlassara, R. Silvestri, A. M. Stefanini, J. F. Smith, D. Steppenbeck, C. A. Ur, P. T. Wady, J. Wrzesiński, E. Maglione, and I. Hamamoto, Phys. Rev. Lett. **102**, 242502 (2009).
[4] S. Szilner, C. A. Ur, L. Corradi, N. Mărginean, G. Pollarolo, A. M. Stefanini, S. Beghini, B. R. Behera, E. Fioretto, A. Gadea, B. Guiot, A. Latina, P. Mason, G. Montagnoli, F. Scarlassara, M. Trotta, G. de Angelis, F. DellaVedova, E. Farnea, F. Haas, S. Lenzi, S. Lunardi, R. Mărginean, R. Menegazzo, D. R. Napoli, M. Nespolo, I. V. Pokrovsky, F. Recchia, M. Romoli, M.-D. Salsac, N. Soić, and J. J. Valiente-Dobon, Phys. Rev. C **76**, 024604 (2007).
[5] A. M. Stefanini, L. Corradi, G. Maron, A. Pisent, M. Trotta, A. M. Vinodkumar, S. Beghini, G. Montagnoli, F. Scarlassara, G. F. Segato *et al.*, Nucl. Phys. A **701**, 217c (2002).
[6] A. Gadea (EUROBALL Collaboration and PRISMA-2 Collaboration), Eur. Phys. J. A **20**, 193 (2004).
[7] Z. M. Wang, R. Chapman, X. Liang, F. Haas, M. Bouhelal, F. Azaiez, B. R. Behera, M. Burns, E. Caurier, L. Corradi *et al.*, Phys. Rev. C **81**, 064301 (2010).
[8] X. Liang, F. Azaiez, R. Chapman, F. Haas, D. Bazzacco, S. Beghini, B. R. Behera, L. Berti, M. Burns, E. Caurier *et al.*, Phys. Rev. C **74**, 014311 (2006).
[9] R. Chapman, A. Hodsdon, M. Bouhelal, F. Haas, X. Liang, F. Azaiez, Z. M. Wang, B. R. Behera, M. Burns, E. Caurier, L. Corradi, D. Curien, A. N. Deacon, Zs. Dombrádi, E. Farnea, E. Fioretto, A. Gadea, F. Ibrahim, A. Jungclaus, K. Keyes, V. Kumar, S. Lunardi, N. Mărginean, G. Montagnoli, D. R. Napoli, F. Nowacki, J. Ollier, D. O'Donnell, A. Papenberg, G. Pollarolo, M.-D. Salsac, F. Scarlassara, J. F. Smith, K. M. Spohr, M. Stanoiu, A. M. Stefanini, S. Szilner, M. Trotta, and D. Verney, Phys. Rev. C **92**, 044308 (2015).
[10] A. Hodsdon, R. Chapman, X. Liang, F. Haas, J. Ollier, E. Caurier, F. Nowacki, M.-D. Salsac, F. Azaiez, S. Beghini *et al.*, Phys. Rev. C **75**, 034313 (2007).
[11] R. Chapman, Z. M. Wang, M. Bouhelal, F. Haas, X. Liang, F. Azaiez, B. R. Behera, M. Burns, E. Caurier, L. Corradi *et al.*, Phys. Rev. C **93**, 044318 (2016).
[12] R. Chapman, Z. M. Wang, M. Bouhelal, F. Haas, X. Liang, F. Azaiez, B. R. Behera, M. Burns, E. Caurier, L. Corradi *et al.*, Phys. Rev. C **94**, 024325 (2016).
[13] Z. M. Wang, R. Chapman, X. Liang, F. Haas, F. Azaiez, B. R. Behera, M. Burns, E. Caurier, L. Corradi, D. Curien *et al.*, Phys. Rev. C **81**, 054305 (2010).
[14] Z. M. Wang, R. Chapman, F. Haas, X. Liang, F. Azaiez, B. R. Behera, M. Burns, L. Corradi, D. Curien, A. N. Deacon, Zs. Dombrádi, E. Farnea, E. Fioretto, A. Gadea, A. Hodsdon, F. Ibrahim, A. Jungclaus, K. Keyes, V. Kumar, A. Latina, N. Mărginean, G. Montagnoli, D. R. Napoli, J. Ollier, D. O'Donnell, A. Papenberg, G. Pollarolo, M.-D. Salsac, F. Scarlassara, J. F. Smith, K. M. Spohr, M. Stanoiu, A. M.

Stefanini, S. Szilner, M. Trotta, and D. Verney, Phys. Rev. C **83**, 061304(R) (2011).
[15] D. O'Donnell, R. Chapman, X. Liang, F. Azaiez, F. Haas, S. Beghini, B. R. Behera, M. Burns, E. Caurier, L. Corradi *et al.*, Phys. Rev. C **81**, 024318 (2010).
[16] Z. M. Wang, Ph.D. thesis, University of the West of Scotland, 2010 (unpublished).
[17] A. Hodsdon, Ph.D. thesis, University of Paisley, 2007 (unpublished).
[18] D. O'Donnell, Ph.D. thesis, University of the West of Scotland, 2009 (unpublished).
[19] E. Caurier, G. Martínez-Pinedo, F. Nowack, A. Poves, and A. P. Zuker, Rev. Mod. Phys. **77**, 427 (2005).
[20] D. Montanari, S. Leoni, D. Mengoni, J. J. Valiente-Doboń, G. Benzoni, N. Blasi, G. Bocchi, P. F. Bortignon, S. Bottoni, A. Bracco *et al.*, Phys. Rev. C **85**, 044301 (2012).
[21] S. Bhattacharyya, M. Rejmund, A. Navin, E. Caurier, F. Nowacki, A. Poves, R. Chapman, D. O'Donnell, M. Gelin, A. Hodsdon *et al.*, Phys. Rev. Lett. **101**, 032501 (2008).
[22] C. Louchart, A. Obertelli, A. Görgen, W. Korten, D. Bazzacco, B. Birkenbach, B. Bruyneel, E. Clément, P. J. Coleman-Smith, L. Corradi *et al.*, Phys. Rev. C **87**, 054302 (2013).
[23] R. Broda, M. Quader, P. Daly, R. Janssens, T. Khoo, W. Ma, and M. Drigert, Phys. Lett. B **251**, 245 (1990).
[24] B. Fornal, R. H. Mayer, I. G. Bearden, P. Benet, R. Broda, P. J. Daly, Z. W. Grabowski, I. Ahmad, M. P. Carpenter, P. B. Fernandez *et al.*, Phys. Rev. C **49**, 2413 (1994).
[25] I. Y. Lee, S. Asztalos, M.-A. Deleplanque, B. Cederwall, R. M. Diamond, P. Fallon, A. O. Macchiavelli, L. Phair, F. S. Stephens, G. J. Wozniak *et al.*, Phys. Rev. C **56**, 753 (1997).
[26] M. Bouhelal, F. Haas, E. Caurier, F. Nowacki, and A. Bouldjedri, Nucl. Phys. A **864**, 113 (2011).
[27] S. Akkoyun, A. Algora, B. Alikhani, F. Ameil, G. de Angelis, L. Arnold, A. Astier, A. Ataç, Y. Aubert, C. Aufranc *et al.*, Nucl. Instrum. Methods Phys. Res., Sect. A **668**, 26 (2012).
[28] L. Grocutt *et al.* (unpublished).
[29] A. Goasduff *et al.* (unpublished).
[30] A. Dewald, in *Ancillary Detectors and Devices for Euroball*, edited by H. Grawe (GSI and the Euroball Ancillary Group, Darmstadt, 1980), p. 70.
[31] G. Montagnoli, A. M. Stefanini, M. Trotta, S. Beghini, M. Bettini, F. Scarlassara, V. Schiavon, L. Corradi, B. R. Behera, E. Fioretto *et al.*, Nucl. Instrum. Methods Phys. Res., Sect. A **547**, 455 (2005).
[32] S. Beghini, L. Corradi, E. Fioretto, A. Gadea, A. Latina, G. Montagnoli, F. Scarlassara, A. M. Stefanini, S. Szilner, M. Trotta *et al.*, Nucl. Instrum. Methods Phys. Res., Sect. A **551**, 364 (2005).
[33] A. Gadea, E. Farnea, J. Valiente-Dobón, B. Million, D. Mengoni, D. Bazzacco, F. Recchia, A. Dewald, Th. Pissulla, W. Rother *et al.*, Nucl. Instrum. Methods Phys. Res., Sect. A **654**, 88 (2011).
[34] F. C. L. Crespi, F. Camera, O. Wieland, G. Benzoni, S. Brambilla, B. Million, and D. Montanari, Nucl. Instrum. Methods Phys. Res., Sect. A **570**, 459 (2007).
[35] A. Lopez-Martens, K. Hauschild, A. Korichi, J. Roccaz, and J.-P. Thibaud, Nucl. Instrum. Methods Phys. Res., Sect. A **533**, 454 (2004).
[36] B. A. Brown and W. A. Richter, Phys. Rev. C **74**, 034315 (2006).
[37] W. A. Richter, S. Mkhize, and B. A. Brown, Phys. Rev. C **78**, 064302 (2008).
[38] E. Caurier and F. Nowacki, Acta Phys. Pol. B **30**, 705 (1999).
[39] E. Caurier, G. Martínez-Pinedo, F. Nowacki, A. Poves, J. Retamosa, and A. P. Zuker, Phys. Rev. C **59**, 2033 (1999).
[40] W. Davies, J. Hardy, and W. Darcey, Nucl. Phys. A **128**, 465 (1969).
[41] S. Khan, G. Mairle, K. T. Knöpfle, T. Kihm, P. Liu-Ken, P. Grabmayr, G. J. Wagner, and L. Friedrich, Nucl. Phys. A **481**, 253 (1988).
[42] J. Chen and B. Singh, Nucl. Data Sheets **112**, 1393 (2011).
[43] W. Currie, L. Earwaker, J. Martin, and A. S. Gupta, Phys. Lett. B **28**, 480 (1969).
[44] A. R. Poletti, T. T. Bardin, J. G. Pronko, and R. E. McDonald, Phys. Rev. C **7**, 1433 (1973).
[45] P. Wagner, J. P. Coffin, M. A. Ali, D. E. Alburger, and A. Gallmann, Phys. Rev. C **7**, 2418 (1973).
[46] W. Andrejtscheff, L. Zamick, N. Marupov, K. Muminov, and T. Muminov, Nucl. Phys. A **351**, 54 (1981).
[47] S. Aydin, M. Ionescu-Bujor, G. T. Gavrilov, B. I. Dimitrov, S. M. Lenzi, F. Recchia, D. Tonev, M. Bouhelal, F. Kavillioglu, P. Pavlov *et al.*, Phys. Rev. C **96**, 024315 (2017).
[48] M. R. Nixon, G. D. Jones, P. R. G. Lornie, A. Nagel, P. J. Nolan, H. G. Price, and P. J. Twin, J. Phys. G: Nucl. Phys. **1**, 430 (1975).
[49] J. Chen, J. Cameron, and B. Singh, Nucl. Data Sheets **112**, 2715 (2011).
[50] K.-H. Speidel, S. Schielke, J. Leske, N. Pietralla, T. Ahn, A. Costin, M. Schmid, O. Zell, J. Gerber, P. Maier-Komor *et al.*, Phys. Lett. B **659**, 101 (2008).
[51] S. Aydin, M. Ionescu-Bujor, F. Recchia, S. M. Lenzi, M. Bouhelal, D. Bazzacco, P. G. Bizzeti, A. M. Bizzeti-Sona, G. de Angelis, I. Deloncle *et al.*, Phys. Rev. C **89**, 014310 (2014).
[52] N. Nica and B. Singh, Nucl. Data Sheets **113**, 1563 (2012).
[53] P. C. Bender, S. L. Tabor, V. Tripathi, C. R. Hoffman, L. Hamilton, A. Volya, R. M. Clark, P. Fallon, A. O. Macchiavelli, S. Paschalis *et al.*, Phys. Rev. C **85**, 044305 (2012).
[54] R. Chapman, M. Bouhelal, and F. Haas (unpublished).
[55] M. Bouhelal, F. Haas, E. Caurier, and F. Nowacki, AIP Conf. Proc. **1491**, 38 (2012).
[56] J. P. Dufour, R. Del Moral, A. Fleury, F. Hubert, D. Jean, M. S. Pravikoff, H. Delagrange, H. Geissel, and K.-H. Schmidt, Z. Phys. A **324**, 487 (1986).
[57] M. Wiedeking, E. Rodriguez-Vieitez, P. Fallon, M. P. Carpenter, R. M. Clark, D. Cline, M. Cromaz, M. Descovich, R. V. F. Janssens, I.-Y. Lee *et al.*, Phys. Rev. C **78**, 037302 (2008).
[58] M. Bouhelal (private communication).
[59] J. Ollier, R. Chapman, X. Liang, M. Labiche, K. M. Spohr, M. Davison, G. de Angelis, M. Axiotis, T. Kröll, D. R. Napoli, T. Martinez, D. Bazzacco, E. Farnea, S. Lunardi, A. G. Smith, and F. Haas, Phys. Rev. C **71**, 034316 (2005).
[60] R. K. Bansal and J. B. French, Phys. Lett. **11**, 145 (1964).